2D/3D Heterojunction Carrier Dynamics and Interface Evolution for Efficient Inverted Perovskite Solar Cells

Abstract

The 2D/3D heterojunction perovskites have garnered increasing attention due to their exceptional moisture and thermal stability. However, few works have paid attention to the influence of the subsequent change process of 2D/3D heterojunction PSC on the stability of PSCs. Moreover, the evolution of the interface and carrier dynamic behavior of the 2D/3D perovskite films with long-term operation has not been systematically developed before. In this work, the effects of 2D/3D heterojunction evolution on the interface of perovskite films and different carrier dynamics during 2D/3D evolution are systematically analyzed for the first time. The decomposition of 2D/3D heterojunction in the perovskite film will have a certain impact on the surface and carrier dynamics behavior of perovskite. During the evolution of 2D/3D heterojunction, PbI_2 crystals will appear, which will improve the interfacial energy level matching between the electron transport layer and perovskite film. With a long evolution time, some holes will appear on the surface of perovskite film. The open circuit voltage (V_{OC}) of PSCs increased from 1.14 V to 1.18 V and the PCE increased to 23.21% after 300 hours storage in the nitrogen atmosphere, and maintained 89% initial performance for with 3000 hours stability test in N_2 box. This discovery has a significant role in promoting the development of inverted heterojunction PSCs and constructing the revolution mechanism of charge carrier dynamic.

Keywords: 2D/3D heterojunction, interface, carrier dynamics, evolution, inverted PSCs.

1. Introduction

The organic-inorganic hybrid halogenated perovskites have attracted much attention due to their favorable photoelectric properties [1-3], and the PCE of perovskite solar cells (PSCs) has risen rapidly from 3.8% [4] in 2009 to exceeding 26% [5] in 2024. Unfortunately, the three-dimensional (3D) is not stable enough due to its own ion migration and phase transitions, which seriously hinders the commercialization of PSCs [6-8]. The two-dimensional (2D) perovskites are stable enough, but the PCE is not that high due to their poor carrier transport ability. Compared with 3D perovskites and 2D perovskites, the 2D/3D heterojunction perovskites have been widely concerned for their good stability and excellent photoelectric properties [9-15].

In the past decade, 2D/3D heterojunction PSCs have undergone significant development [16,17] and various preparation methods of 2D/3D heterojunction perovskite have been proposed, such as bulk phase doping [18,19], surface treatment [20] and vapor deposition [21] methods. One of the most promising ways to constructing 2D/3D heterojunction is spin-coating organic spacer molecules on top of 3D perovskite film [22,23]. Meanwhile, the residual organic spacers will affect the electronic properties of 2D/3D heterojunction interface [24]. Furthermore, the presence of 2D/3D heterojunctions can also suppress the degradation of 3D perovskite crystals in air environmental conditions [25]. When the perovskite film is affected by both water and heat, the water molecules can only penetrate 3D perovskite film after the 2D perovskite layer disappears, which resulting in the degradation and phase transition of 3D perovskite [26]. At the same time, in situ X-ray scattering experiments at the 2D/3D interface, 3D perovskite crystals dynamically transformed into 2D/3D mixed phases and hindered the degradation of 3D perovskite to PbI_2 [27]. Therefore, constructing 2D/3D heterojunctions in perovskites can effectively improves the crystallization of 3D perovskites by adding 2D perovskites [28], enhances carrier transport ability by constructing 2D passivation layer on the upper interface of 3D perovskites [29], improves charge extraction efficiency and reduces non-radiative recombination by constructing 2D perovskites on the bottom interface of 3D perovskites [30,31]. Although 2D/3D

heterostructure synthesizes the performance advantages of both sides, the degradation and transition mechanisms of 2D and 3D are different, which will inevitably affect the photoelectric conversion performance of PSCs.

3D perovskites are susceptible to phase transitions and degradation caused by moisture, light, and temperature in the environment due to its special crystal structure [32]. In the phase structure of 3D perovskites, the black alpha phase perovskites exhibit strong light absorption capacity, while the yellow delta phase perovskites exhibit poor photovoltaic effect [33]. At the same time, the alpha phase of 3D perovskite spontaneously transitions to the delta phase because of ion migration within the perovskite crystal, the accumulation of defect states, and the rotation and tilt of the lead iodide octahedron [PbI_6] [34]. When perovskite is placed under long-term light, perovskite will destroy the cubic phase crystal due to its own ion migration. In addition, perovskite is sensitive to humidity, and hydrolysis reaction is easy to occur in high humidity environment [35,36]. The long-term heating can also lead to the degradation of perovskite, because heating will produce some active substances to destroy the original stable cubic structure of perovskite [37,38]. Meanwhile, the 2D perovskites consist of alternating layers of organic cation spacers and inorganic frames [39]. Compared to 3D perovskites, the 2D perovskites can exhibit more stable performance in humidity and moisture environments because their layered structure reduces the penetration and influence of water molecules [40]. However, even though 2D perovskites are more stable in high humidity and moisture environments, hydrolysis reactions can still occur in extremely humid environments [33]. In long-term thermal stability tests, the 2D perovskites also showed excellent performance compared to 3D perovskites, but the 2D perovskites still degrade at higher temperatures due to thermal stress [41]. Among them, the degradation of 2D perovskite is mainly caused by cationic evaporation under the action of thermal stress [42,43]. In addition, the rigidity and heat resistance of organic spacer molecules used to construct 2D perovskites will also affect the stability and thermal decomposition ability of 2D perovskites [44]. In the process of long-term stable operation of perovskite, 3D perovskite and 2D perovskite crystals will degrade due to the influence of external environmental factors, thereby reducing the photoelectric

capacity of perovskite. However, there are few studies on the subsequent evolution process of 2D/3D heterojunction interfaces and charge carrier dynamic behavior with the evolution of 2D/3D heterojunction perovskite [45]. In addition, many studies have shown that the stability of perovskite solar cells built with 2D/3D heterogeneous structures has been greatly improved [46], and the final stability improvement of PSCs is due to the existence of 2D perovskite, which inhibits the interface defects [47,48]. However, few people pay attention to the influence of the subsequent change process of 2D/3D heterojunction PSC on the stability of PSCs. A better understanding of the carrier dynamics of this evolution is of great significance for the development of 2D/3D heterojunctions.

In this work, the 2D/3D heterojunction perovskite films were placed on the heating table at 60℃ to accelerate the evolution process. With time going, a series of changes will occur on the surface of 2D/3D perovskite films, and it is easier to find the changes of 2D decomposed surface morphology and carrier dynamics. By studying the changes of 2D/3D perovskite interface, we can more clearly understand the effects of 2D/3D heterojunction evolution behavior. Finally, the dynamic behavior of 2D/3D perovskite films during evolution is compared. The surface variation and carrier dynamics of perovskite thin films are important factors affecting the stability of PSCs.

2. Test results and analysis

2.1 Evolution of perovskite films

In this experiment, the one-step reverse-solvent engineering was used to fabricate inverted perovskite solar cells (PSCs) initially. Firstly, as illustrated in Fi**g. S1**, the electrostatic potential of PEABr molecular structure is analysed by using the Gaussian view in an ideal state without considering the influence of other external factors. The results show that the Br^- containing end exhibits a notably intense signal of negative charge region signal, suggesting that the Br^- containing branch chain has a stronger attraction towards positively charged ions within PEABr molecules. However, the benzene ring shows positive charge accumulation, and the nitrogen atom in the side chain shows stronger positive charge accumulation. This indicates that both the benzene

ring and the nitrogen atom have a stronger binding affinity for negatively charged ions.

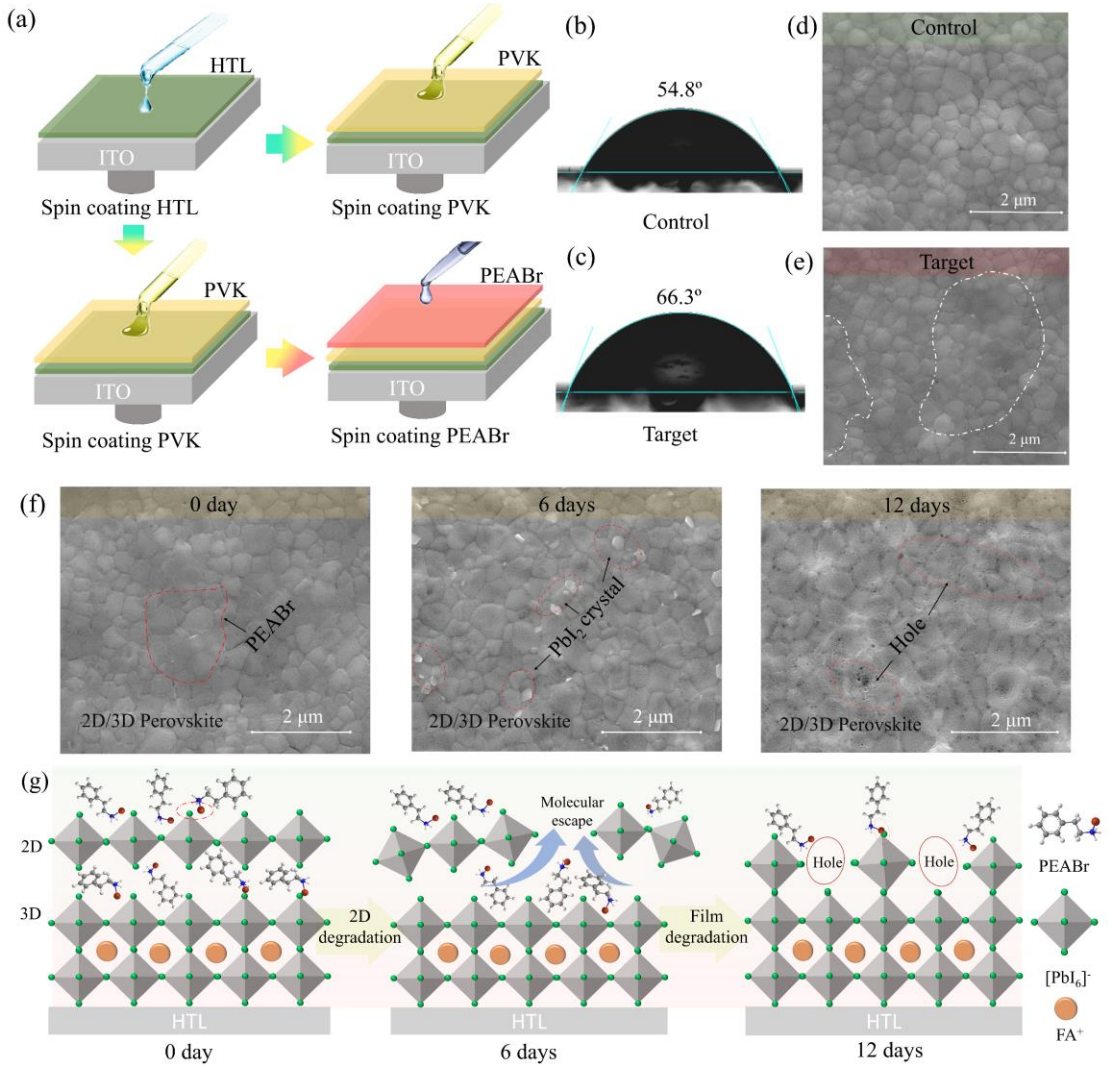

Figure 1. (a) Schematic diagram of perovskite film construction by different method. (b) Contact angle test diagram of perovskite film of control. (c) Contact angle test diagram of perovskite film of control target. (d) SEM image of perovskite film of control. (e) SEM image of perovskite film of target. (f) Surface diagram of perovskite films with target film placed on a hot table at 60℃ for different storage times. (g) schematic diagram of the 2D/3D interface change process of target perovskite film on the hot table at 60℃ for different time.

As shown in **Fig. 1a**, this is the process of experimentally constructing the 2D/3D heterojunction by spinning a layer of PEABr on the upper surface of 3D perovskite. This organic cation on the upper surface of the 3D perovskite will cause the 3D perovskite to be transformed into a low-dimensional perovskite. In the figure, films that are not coated with PEABr are labeled as the control, while the films coated with PEABr

are labeled as the target. In the process of constructing the 2D/3D heterojunction, compared with the control film, there is a special phenomenon after the PEABr spin coating on the upper surface of the perovskite film, which showed a colored halo of the perovskite film. Then, the contact angle test was conducted on the perovskite film to explore the impact of 2D/3D heterostructures and residual PEABr on the upper surface of both the control perovskite and the target perovskite films on the subsequent spin coating process. It can be seen from **Fig. 1d** and **1e** that the contact angle of the control perovskite film is 54.8°, while the target perovskite film is 66.3°. The water contact angle of the 2D/3D heterojunction after being constructed with PEABr shows an improvement of 11.5°. This indicates that the residual PEABr and the 2D/3D heterojunction on the upper surface of 3D perovskite improved the hydrophobicity of the film and adjusted the interface morphology of the film. At the same time, a humidity stability test of the perovskite film was conducted at 25℃ and 45%RH (**Fig. S2**). The results indicated that the surfaces of both the target film and the control perovskite film did not exhibit significant changes after 1000 hours of storage. However, in comparison to the control perovskite film, the colour of the edge of the target perovskite film has changed significantly, which we believe is caused by the residual PEABr on the surface of the perovskite. The scanning electron microscopy (SEM) test results, as shown in **Fig. 1d and 1e**, reveal that the grain size of both the target and control perovskite films was similar. However, there were significant gaps between the grains in the control film, making it easier for PEABr to react with the 3D perovskite. Moreover, these voids will also cause PEABr molecules to gather around them. It can be clearly seen in the test results that there are some residual PEABr molecules in the target perovskite film grain gaps. At the same time, the SEM test results of various scales and positions of perovskite films in **Fig. S3** indicate that this phenomenon is not unique. This phenomenon also demonstrates that the surface adhesion of residual PEABr molecules on 2D/3D perovskite plays a role in passivating interface defects, as characterized through further analysis. Then, as shown in **Fig. S4**, to investigate the thermal stability of the perovskite films, both the control and target perovskite films were subjected to continuous heating on a hot plate at 60℃. It can be observed that the perovskite in the

control film has essentially decomposed after 1400 hours, whereas the target film shows a certain black phase after the same duration, indicating greater stability in the target perovskite film. In addition, an unidentified substance precipitated on the upper surface of the target perovskite film after 300 hours. The presence of this unidentified substance suggests that the 2D/3D heterojunction of perovskite has changed during long-term stable operation, which may be caused by the decomposition of the 2D perovskite and the residue of PEABr molecules on the surface of perovskite. This phenomenon offers an opportunity to investigate the evolutionary mechanisms of the 2D/3D heterostructure perovskite films during extended operational periods. Therefore, we can summarize an evolutionary mechanism by conducting tests and characterizations on the 2D/3D heterostructure perovskite films with varying annealing durations.

As shown in **Fig. 1f**, the residual PEABr molecules exist on the upper surface of the fresh (0 day) perovskite film. From the top view of the perovskite film, there are some incomplete substances in the grain gap of perovskite. Moreover, after the same piece of perovskite film was placed on the heating platform for 6 days, some white bright parts appeared in the top view of the SEM, which was proved to be PbI_2 in the previous literature. With the increase of time, the PbI_2 disappeared in the SEM top view of the target perovskite film after 12 days annealing. The lead iodide present during the decomposition of the 2D perovskite may interact with the original FA^+ and PEA^+ ions. At the same time, it can be clearly found that more tiny holes appear on the upper surface of the perovskite film after 12 days of placement, and the grain size of the perovskite film hardly changes during the placement process, which means that the evolution process of the 2D/3D perovskite is beneficial to the crystal stability of the 3D perovskite. Through subsequent characterization tests, a structural evolution process of the upper surface of perovskite films was proposed (**Fig. 1g**). After the target perovskite film is left for 6 days, the 2D perovskite within the 2D/3D heterojunction film will gradually transform. The lead iodide will start to appear on the surface of the film, and PEABr molecules from inside the perovskite will migrate to the surface as the annealing process continues. Over time, the lead iodide appearing on the surface of the perovskite film is covered by the PEABr molecules or reacts with the 3D perovskite at the bottom,

and the PEABr molecules appearing on the upper interface of the perovskite will continue to play an interface passivation effect on the interface of the perovskite. This corresponds to the stability test results in the following section.

2.2 Evolution of perovskite carrier dynamics

The study of carrier transfer kinetics in 2D/3D perovskite films using femtosecond transient absorption spectroscopy (fs-TA) is crucial for comprehending enhancements in their photoelectric properties. **Fig. 2a-2c** and **Fig. S5a** are two-dimensional false-color images of perovskite film on quartz glass substrate with laser excitation of 700 nm, pump flow of 5 $\mu J \cdot cm^{-2}$, and carrier density of 1.34×10^{17} cm^{-3}. The spectra of the four samples show a ground-state bleaching (GSB) centered at 1.58 eV. This bleaching feature indicates that the carrier in the perovskite film transitions from the ground state to the excited state under laser excitation, causing the light absorption difference ΔA to change significantly on a ps scale due to the pumping process. As shown in **Fig. 2a–2c**, it can be found that the duration of bleaching region of the 2D/3D heterostructure perovskite films does not change significantly. Moreover, the variation range of the light absorption difference ΔA of the samples at different placement times is small, and it also indicates that the decomposition of 2D/3D heterojunction has a certain protective effect on 3D perovskite. The **Fig. 2d-2f** and **Fig. S5b** show the normalized time spectra of the control and target perovskite films in the time delay range of 0.4 ps to 10 ps. We found that both the control and the 2D/3D heterojunction perovskite film have a distinct 750-800 nm high-energy tail region (marked in blue) in the TA spectrum, which also reflects the cooling process of the hot carrier. It is noteworthy that the high-energy tail shrinkage rate of 2D/3D heterojunction perovskite films is faster than that of control films, which indicates that 2D/3D heterojunction changes the carrier cooling dynamics in perovskite films.

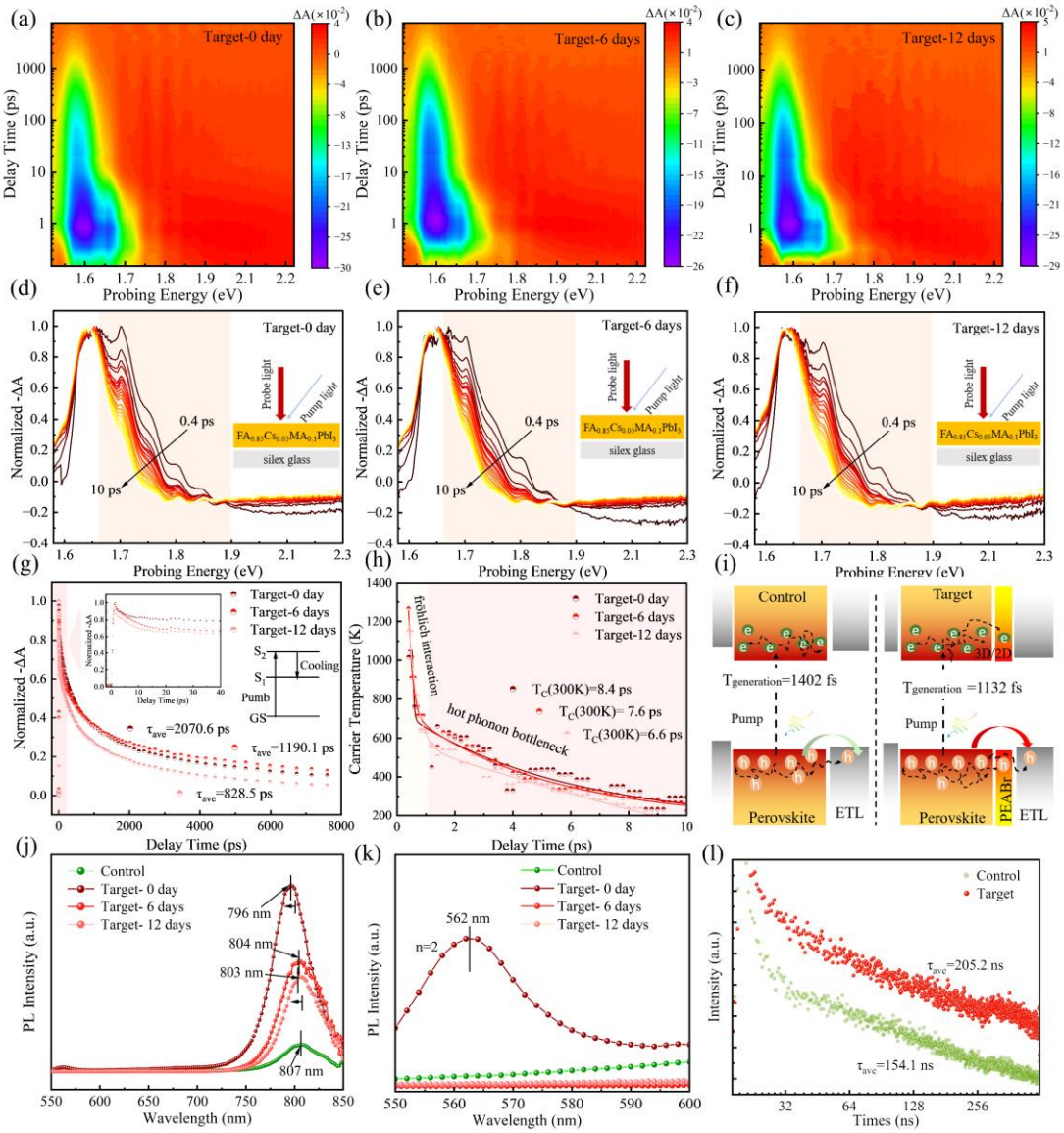

Figure 2. Fs-TA measurements of the 2D/3D perovskite films. (a-c) Two-dimensional false-color image of TA spectral perovskite film on a hot table at 60℃ for different time. (d-f) The TA spectra recorded at several delay times from 0.4 to 10 ps. (g) The corresponding normalized attenuation kinetics curve at 788 nm. (h) Hot carrier cooling time curve of target perovskite film. (i) The interface is between the schematic diagram of electron generation and extraction HTL and Perovskite. (j) PL spectra of control and target perovskite films with different storage times on 60℃ hot table. (k) PL spectra of control and target perovskite films with 550-600 nm wavelength. (l) TRPL spectrum of perovskite films with ITO substrate.

Fig. 2g and **Fig. S5c** show the carrier dynamics curves of perovskite thin films obtained from the highest point of excitation signal. The fitting results obtained by the three-exponential function fitting method on the data in the figure are shown in **Tab.**

S1. At a delay time of 1 ns, the normalized decay rate (ΔA) of the initial 2D/3D perovskite was only 65.17%, while the control perovskite film reached 72.38%. The ΔA of target-6 days perovskite is only 64.38%, compared to 73.61% for target-12 days perovskite films. 2D/3D perovskite films show a higher charge density and slower decay rate. In addition, TA decay can be well fitted using a three-exponential fitting model, and the corresponding parameters are listed in **Tab. S1**. Compared to a pure 3D perovskite with a charge recomposite life of 840.8 ps, the 2D/3D perovskite has a longer life, with a target-0 day of 2070.6 ps, target-6 days of 1190.1 ps, and target-12 days of 828.5 ps. The carrier lifetime of 2D/3D perovskites is longer, indicating that 2D perovskites can reduce the density of defect states and effectively manipulate carrier transfer. At the same time, the evolution process of 2D/3D also influences the defect state and charge transport of perovskite. In the range of 0-1ps, the excitation process of perovskite thin film is displayed, and the target is almost the same as that of perovskite thin film, and the target is almost the same as that of controlling the excitation strength of perovskite thin film. However, it can be clearly seen that the carrier dynamics of the target device changes more slowly during the subsequent carrier cooling process. This means that the carrier lifetime and carrier transport behavior change. Moreover, these high-energy tails gradually disappear from 0.4 ps to 10 ps, suggesting that the hot carrier cooling process in these samples can be evaluated by a hot carrier temperature (Tc) higher than the perovskite lattice temperature. By fitting the high-energy region (red background region) of the above fs-TA spectrum with the following Maxwell-Boltzmann distribution function (formula 1 and 2), the relationship between the hot carrier cooling time and the contraction rate of the high-energy tail can be obtained [49]:

$$\Delta T(\mathrm{h}\omega) = -T_0 exp\left(\frac{E_F - h\omega}{k_B T_c}\right) \quad \text{(formula 1)}$$

$$\Delta A = -log\left(1 + \frac{\Delta T}{T}\right) \quad \text{(formula 2)}$$

where E_F is the Fermi level, ΔT is the amplitude of bleaching at a specific detection wavelength, ΔA is the difference in light absorption at a specific detection wavelength, and k_B is the Boltzmann constant. The initial temperature of the hot carrier depends on the photoexcitation energy, which can be found in some previous studies [49]. Since the

wavelength and energy of the initial excitation laser are fixed, the relationship between the temperature of 2D/3D heterojunction perovskite hot carrier and the delay time can be determined by formulas 1 and 2. **Fig. 2h** and **Fig. S5d** show the change curve of carrier temperature (T_C) with delay time for perovskite films without and with 2D/3D heterojunction. The initial T_C of the control perovskite film is about 1511 K, and the initial T_C of 2D/3D perovskite film is about 1016 K, indicating that 2D perovskite can change the T_C cooling kinetics of 3D perovskite film. The initial T_C of 2D/3D perovskite film placed on a 60℃ hot table for 6 days is about 1266 K, and the initial T_C of 2D/3D perovskite film placed on a 60℃ hot table for 12 days is about 1147 K. All four perovskite films exhibit significant Tc decline, which is due to the ultrafast energy loss of perovskite films through the e carrier-LO-phonon scattering process on several ps time scales. The hot carrier motion behavior of perovskite thin films on the 1 ps time scale corresponds to fast carrier cooling via Fröhlich interaction [50]. The decrease in the thermal carrier temperature relaxation rate represented by another slow cooling process (1-10 ps) after the initial 1 ps attenuates is due to the hot phonon bottleneck effect. The carrier temperature of the 2D-free perovskite film attenuates from 1511 K to 1043 K over a 1 ps time scale, and does not attenuate to 300 K until 8 ps. The carrier temperature of the initial 2D/3D perovskite film attenuate from 1016 K to 639 K on a 1 ps time scale, and does not attenuate to 300 K until 8.4 ps. The 6 days 2D/3D perovskite film attenuates carrier temperatures from 1266 K to 634 K on a 1 ps time scale, and does not attenuate to 300 K until 7.6 ps. The 12 days 2D/3D perovskite film's carrier temperature attenuate from 1147k to 640 K on a 1 ps time scale, and does not attenuate to 300 K until 6.6 ps. Therefore, it can be concluded that the hot carrier cooling of 2D/3D heterojunction perovskite films requires more time, and the increase of hot carrier cooling time indicates that the carriers inside 2D/3D heterojunction perovskite have less energy loss during transport. Compared with the initial 2D/3D perovskite film, the hot carrier cooling time of the perovskite film placed for 6 days is longer, but the hot carrier cooling time of the perovskite film placed for 12 days is only 6.6 ps. Therefore, it can be concluded that more time is required for hot carrier cooling of the 2D/3D heterojunction films, and the increase in hot carrier cooling time indicates

that the carriers inside 2D/3D heterojunction perovskites have less energy loss during transport. **Fig. 2i** shows the excitation time diagram of perovskite film. The photoexcitation process of perovskite film can be obtained from the dynamics diagram of perovskite carrier. The excitation time of perovskite film of free-2D is 1420 fs, and after modification by PEABr, the excitation decay time of perovskite film is reduced to 1132 fs. Pump photoexcitation of the upper surface of perovskite, due to the presence of 2D, makes the overall carrier excitation time shorter, which means that the internal carrier excitation due to 2D/3D perovskite films is easier. For the subsequent electron extraction and transport process, the presence of 2D perovskite changes the energy level and morphology of the perovskite interface, making electron transport easier. It can be found from the carrier dynamic map that the carrier decay time of 2D/3D perovskite is longer than that of non-2D perovskite films, because 2D perovskite improves the interface defects of 3D perovskite. At the same time, the overall attenuation process of the carrier dynamics curve is also affected by the evolution process of 2D/3D heterojunction, which makes the carrier change more slowly. Then, as shown in **Fig. 2j** and **Fig. 2k**, the Photoluminescence spectroscopy (PL) tests were performed on target perovskite films with different storage times. The test results show that the fresh target perovskite film has an obvious low-dimensional perovskite peak of n=2 at the wavelength of 562 nm. Meanwhile, the main peak of the fresh (0 day) perovskite at the wavelength of 800 nm has a blue shift, and the main peak of the target perovskite film moved to a lower wavelength direction than the main peak of the control film. This indicates that the residual PEABr and the 2D/3D heterojunction has interfacial passivation effect on perovskite films. With the increase of the storage time, the peaks belonging to 2D perovskite disappeared, and the peaks of the target perovskite film began to slowly move to a higher wavelength, which indicate that the passivation effect of PEABr was gradually weakened. The perovskite peaks of the fresh (0 day) target perovskite films were significantly higher than those of the control films, suggesting that the non-radiative recombination in the 2D/3D heterojunction perovskite films was effectively inhibited. At the same time, after the target perovskite film is placed on the heating table for different time, the main peak of perovskite shows a downward trend,

which means that the evolution process of the 2D/3D heterojunction influences the interface characteristics of perovskite. As shown in **Fig. 2l**, time-resolved photoluminescence spectroscopy (TRPL) was conducted on the 2D/3D heterojunction perovskite films to investigate their carrier lifetime. The detailed test results can be found in the **Tab. S2**. In general, the fast decay lifetime (τ_1) can be attributed to defect-induced non-radiative recombination, while the slow decay lifetime (τ_2) is associated with radiative recombination. Control and 2D/3D perovskite films have fast decay life (τ_1=6.3ns, τ_1=19.2ns) and slow decay life (τ_2=158.5ns, τ_2=211.2ns), the average carrier lifetime (τ_{ave}= 154.1ns, τ_{ave}= 205.2ns) can be seen the defect and charge recombination in perovskite. The significant increase of fast decay life and slow decay life means that the defect state density decreases significantly and the non-radiative charge recombination decreases. The increase in average carrier lifetime suggests that carriers in the 2D/3D heterojunction perovskite films can travel longer distances, and non-radiative recombination within these films is effectively suppressed, consistent with the PL test findings.

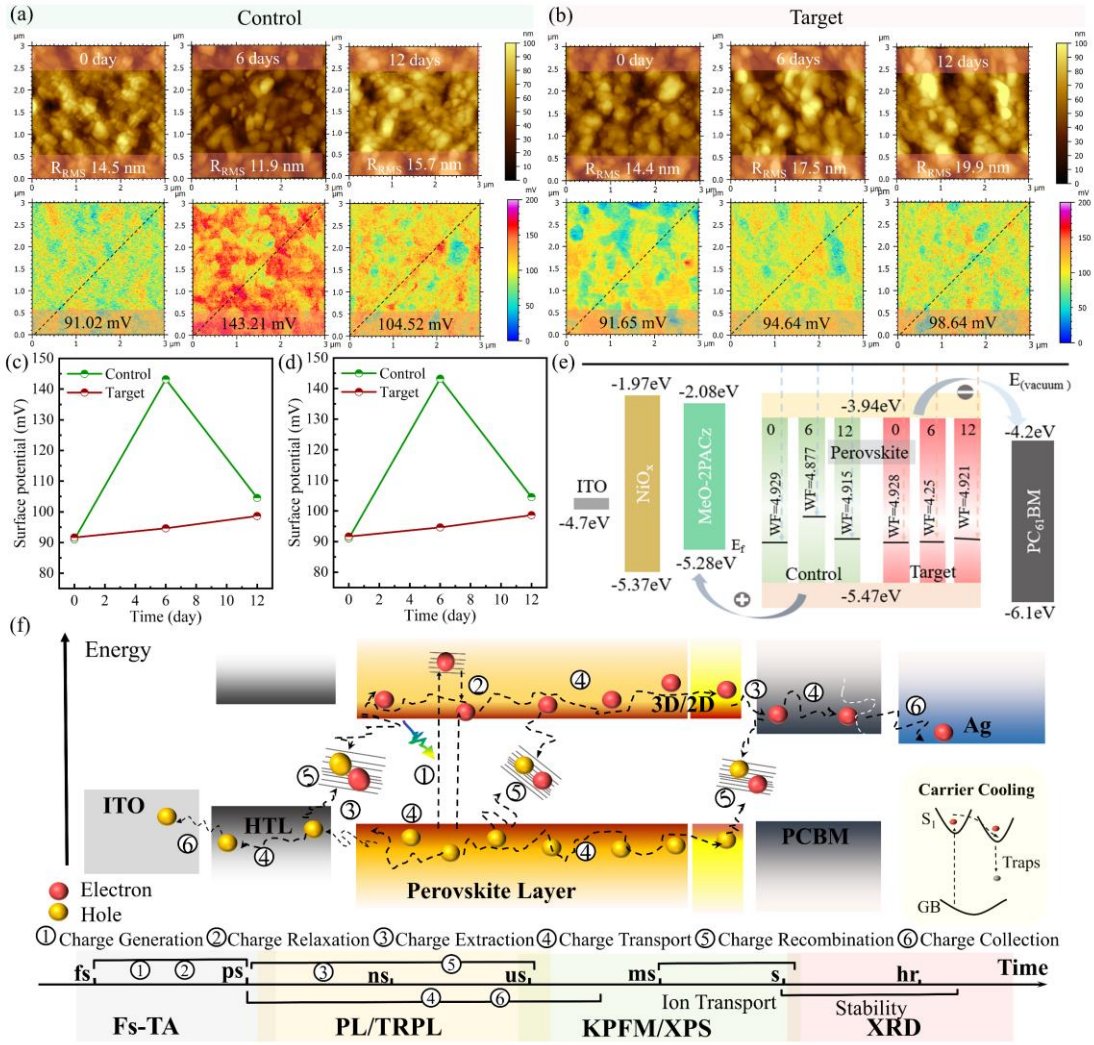

Figure 3. (a) AFM and KPFM diagram of control sample on a hot table at 60℃ for different time. (b) AFM and KPFM diagram of target sample on a hot table at 60℃ for different time. (c) RRMS profiles of control and target perovskite films. (d) Surface potential spectrogram of control and target perovskite films. (e) Work function variation diagram of control and target perovskite film. (f) Simulation diagram of carrier dynamic process and time scale behavior of perovskite.

Afterward, to further verify the process of surface change of the perovskite film, the atomic force microscopy (AFM) and kelvin probe force microscopy (KPFM) were used to test the perovskite film, as shown in **Fig. 3a** and **3b**. The root mean square (R_{RMS}) roughness data of the 2D/3D heterogeneous perovskite films with different heating times were obtained. The R_{RMS} difference between the control and target perovskite films (0 days) was not significant. However, the difference of R_{RMS} values between target film and control film further verified the existence of residual PEABr

and 2D perovskite on perovskite. The control perovskite film exhibited an R_{RMS} of 14.5 nm at 0 days, 11.9 nm at 6 days, and 15.7 nm at 12 days of storage. Conversely, the control perovskite film showed an R_{RMS} of 14.4 nm at 0 days, 17.5 nm at 6 days, and 19.9 nm at 12 days of storage. Meanwhile, the surface roughness of the control perovskite film after 12 days showed no difference compared to the film at 0 days, while the surface roughness of the target perovskite film increased gradually. However, the R_{RMS} value on the upper surface of the target perovskite film changes more gradually compared to the control perovskite film, significantly impacting the stability of PSCs. This observation, coupled with previous test results, suggests that it may be attributed to the decomposition of 2D perovskites and the emergence of PbI_2 crystals, influencing the surface characteristics of the 2D/3D heterojunction perovskites. At the same time, the KPFM testing indicated minimal difference in surface potential between the upper surface of the freshly prepared (0 day) control and target perovskite films (data from the diagonal). However, it could be seen from the analysis of the overall image that the upper surface potential of the target perovskite film was more concentrated, which may be caused by the presence of residual PEABr and the 2D/3D heterojunction perovskite. Meanwhile, the residual PEABr and the 2D/3D heterojunction perovskite fill the low potential space at the original 3D perovskite interface, which makes the potential on the surface of the perovskite appear more uniform. Additionally, the KPFM test was conducted on a perovskite film placed on a 60°C hot platform for different time. While the surface potential of the control films exhibited significant fluctuations over time, that of the target perovskite films remained largely unchanged. The surface potential and R_{RMS} of the target perovskite film exhibited a gradual increasing trend, while those of the control perovskite film showed a pattern of initially decreasing and then increasing. As shown in **Fig. 3c**, the surface R_{RMS} changes of target and control perovskite films show a more gradual change in the surface R_{RMS} of 2D/3D perovskite films compared with control films. The surface potential variation diagram of the control and target perovskite film is shown in **Fig. 3d**. The surface potential of the control film fluctuates greatly. **Fig. 3e** shows the relationship between the surface work function and the energy band change of the control and target perovskite films. Since

the 2D content of the target perovskite film is very small, the energy level of the target perovskite is tentatively like that of the control perovskite film. Excessive fluctuation in the upper surface of the perovskite film during the 12 days placement period can be detrimental to the final PSCs stability. Around 6 days of the target device, the slow increase in surface potential and R_{RMS} may be linked to the evolution of the 2D/3D heterojunction, influenced by the appearance of PbI_2 crystals and the decomposition of 2D perovskite, potentially compensating for perovskite film defects. **Fig. 3f** shows the entire carrier dynamic behavior relationship of perovskite. The behavior of photoexcited carrier between the interface of perovskite is affected by the defects in the perovskite and the carrier transport path. The carrier in perovskite film will undergo non-radiative recombination between perovskite film and perovskite interface, resulting in the quenching of the carrier. The carrier transport between interfaces will also be affected by the defect states and the energy level matching relationship between the interfaces. Therefore, the evolution of 2D/3D heterojunction is related to the behavior of perovskite carrier dynamics. Carriers transition from the ground state to the excited state by optical excitation, and then naturally return from the excited state to the ground state or are trapped by defects. This process of high-energy carrier return to the ground state can be described by carrier cooling. Because the process of carrier generation and transfer occurs very quickly, it will show different dynamics at different time scales. We use corresponding test methods to study the evolution of 2D/3D heterojunctions and the dynamic behavior changes of charge carriers. The evolution process of 2D/3D heterojunction has great influence on the stability of perovskite, and the fluctuation of perovskite interface can cause the change of carrier dynamics.

2.2 Analysis of perovskite films and devices

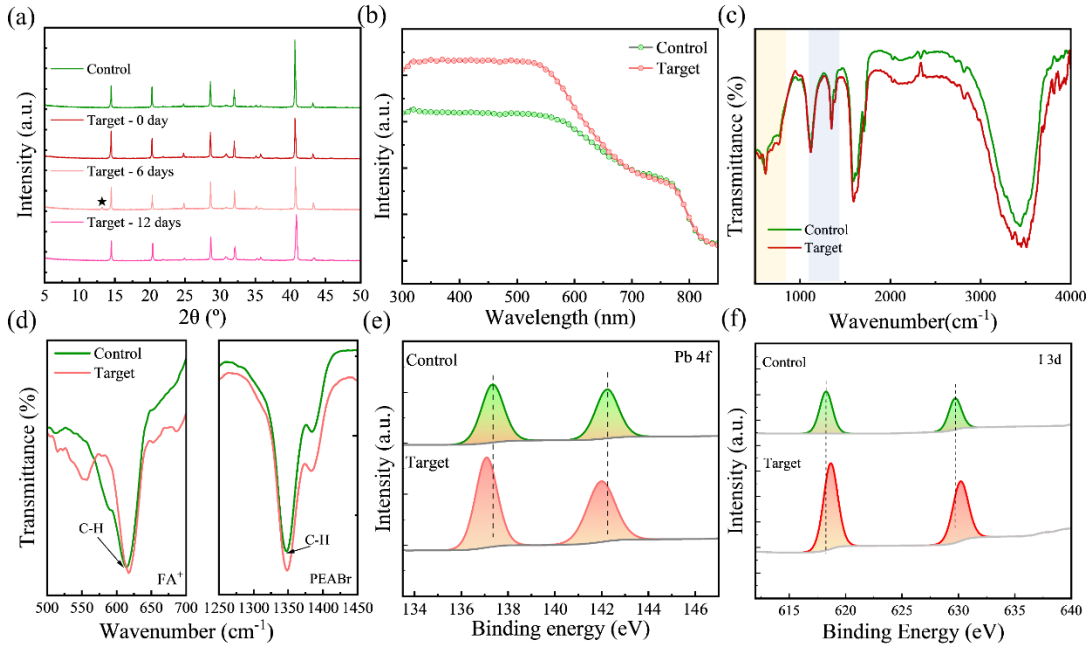

Figure 4. (a) XRD diagram of control and target perovskite films placed on the 60°C hot platform for different times. (b) UV-vis absorption spectra of perovskite films with ITO substrate. (c) FTIR diagram of perovskite films with ITO substrate. (d) FTIR diagram of perovskite films with 500 cm^{-2} to 1500 cm^{-2} wavenumber. (e, f) XPS diagram of perovskite films with ITO substrate.

To investigate the changes that occur on the surface of perovskite films during extended annealing processes, perovskite films with varying annealing durations underwent X-ray diffraction (XRD) tests (**Fig. 4a**). On the initial day (0 day), the target perovskite film demonstrates a more pronounced signal at the α phase peak of 14.5° in contrast to the control film. This suggests that the α phase perovskite crystals in the target film are more oriented along the (001) direction. The better crystallization of the perovskite also indicates that the presence of the 2D/3D heterojunction can better protect the crystals inside the 3D perovskite. At the same time, the δ phase diffraction peak intensity of the target film at 42° is lower than that of the control perovskite film, which indicates that the presence of the 2D/3D heterojunction can improve the stability of 3D perovskite phase. The film subjected to 60°C on a hot platform for 6 days simultaneously exhibited a weak PbI_2 peak at 12.4°, consistent with SEM results. As storage time increased, the PbI_2 peak diminished, while the δ phase peak continued to decrease. The observed PEABr escape during storage appears beneficial for the overall

perovskite film. Furthermore, the stability of the target perovskite film (001) peak suggests that PEABr escape does not significantly affect the bulk phase of the perovskite. Subsequently, the ultraviolet-visible (UV-vis) spectrophotometer tests were conducted on the control and target perovskite samples. As shown in **Fig. 4b**, the visible light absorption range of the target perovskite film is lower than that of the control perovskite film. This disparity may arise from alterations in the band gap of the target perovskite film due to the presence of the 2D perovskite and residual PEABr. Then, as shown in **Fig. S6**, the optical band gap of both the control and target films was calculated using ultraviolet data. The results indicate that the optical band gap of the perovskite film increases from 1.524 eV to 1.529 eV due to the presence of the 2D perovskite and PEABr. However, between 300 nm and 550 nm, the visible light absorption capacity of the target film shows a notable improvement compared to the control film, indicating a reduction in non-radiative recombination in the surface of the target perovskite film. At the same time, the 2D perovskite can improve the band gap of perovskite, which has been demonstrated in previous studies. Ziqi Liang et al found that the band gap of the 2D perovskite is usually higher than that of the 3D perovskite solar cells [37]. Therefore, for two-dimensional passivation layers prepared with PEABr, it is a normal phenomenon that the band gap of perovskite films is improved. The increase in the perovskite band gap also provides direct evidence for the increase in the open circuit voltage (V_{OC}) of the final device. To further investigate the changes in internal bonding atoms within the control and target perovskite films, Fourier-transform infrared spectroscopy (FTIR) was conducted, as depicted in **Fig. 4c**. It can be found that the N-H stretching vibration absorption wavelength in perovskite moves from 3440 cm^{-1} to 3515 cm^{-1}, while the vibration absorption wavelength of C=N moves from 1590 cm^{-1} to 1596 cm^{-1}. The wavelength of N-H and C=N bond moves to higher wavelength, which indicates that PEABr has certain induction effect on perovskite molecules in perovskite films. The **Fig. 4d** shows the low wave number amplification in the FTIR graph. From the test results, it can be inferred that the bending vibration absorption wavelength of the C-H bond in the perovskite component ranges from 615 cm^{-1} to 617 cm^{-1}, whereas the bending vibration absorption wavelength of the C-H bond in PEABr

ranges from 1347 cm^{-1} to 1349 cm^{-1}. The C-H bond in the FA^+ and the C-H bond in the PEABr oscillate simultaneously, indicating the interaction between PEABr and FA^+. At the same time, as shown in **Fig. 4e** and **4f**, X-ray photoelectron spectroscopy (XPS) analysis was conducted on the target and control perovskite films to investigate changes in element binding energy peaks on their surfaces. The fitting results revealed that in the target perovskite film, the Pb^{4f} peak shifted towards lower binding energy, suggesting that the presence of PEABr altered the environment surrounding Pb ions, promoting their binding with FA^+. The shift of the I^{3d} peak towards higher binding energy in the target perovskite film indicates reduced reactivity of I ions within the perovskite structure, thereby potentially lowering the defect density attributed to iodine ions. Combining the previous FTIR test results and the molecular electrostatic potential results of PEABr, the PEA^+ ions can interact with I element, thus affecting the existence form of I element, and the Br^- can interact with Pb element, thus changing some of the action characteristics of Pb element. Meanwhile, the full peak of XPS test results is shown in **Fig. S7**. Since the control film does not contain Br element, the content of Br element in the target film is very small, so there is no strong peak of Br element in the XPS test results. These phenomena further show that the evolution process of the 2D/3D heterojunction is regular. In previous the 2D/3D studies it was found that 2D perovskites constructed using some special organic spacer molecules would diffuse to 3D perovskites. This diffusion process destroys the crystal structure of the 3D perovskite and causes severe ion migration and defect aggregation in the 3D perovskite. In this experiment, the 2D passivation layer constructed by the PEABr on the upper surface of the 3D perovskite will decompose and the PEABr molecules will separate on the upper surface of the perovskite film over time, because the characteristics of Br^- make it migrate to the upper surface of perovskite during the process of ion migration.

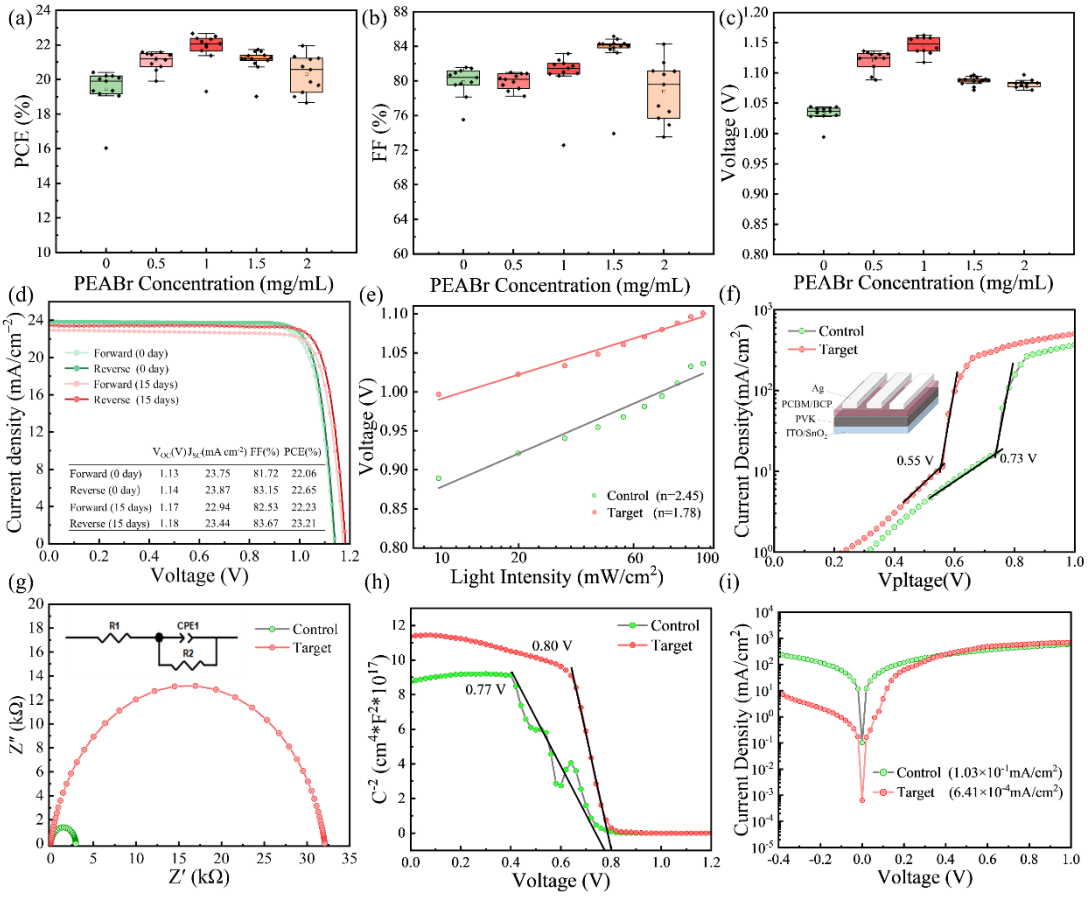

	V_{OC}(V)	J_{SC}(mA cm^{-2})	FF(%)	PCE(%)
Forward (0 day)	1.13	23.75	81.72	22.06
Reverse (0 day)	1.14	23.87	83.15	22.65
Forward (15 days)	1.17	22.94	82.53	22.23
Reverse (15 days)	1.18	23.44	83.67	23.21

Figure 5. (a-c) Photovoltaic performance diagram of control and target devices. (d) J-V diagram of 0.105 cm^2 fresh device and after 15 days device in N_2 boxes at normal temperature. (e) Light intensity dependence test diagram between control and target devices. (f) SCLC test diagram of control and target devices. (g) EIS diagram of the control and target devices. (h) Mott-Schottky diagram of control and target devices. (i) Dark current test diagram of control and target devices.

In this experiment, the final prepared device structure is shown in supplementary **Fig. S8.** By spinning PEABr on the upper surface of 3D perovskite as the passivation interface layer of perovskite, the PEABr can construct 2D perovskite layer on the upper surface of 3D perovskite and form the 2D/3D heterostructures. The 2D/3D heterojunction PSCs constructed using this method have significantly improved performance and stability compared to pure 3D perovskite. First, as shown in **Fig. 5a-c** and supplementary **Fig. S9**, the open circuit voltage (V_{OC}) and fill factor (FF) of the target device with the PEABr and the 2D/3D heterojunction are greatly improved. The highest PCE of the prepared 0.105cm^2 PSCs reaches 22.65% (the detailed data are shown in **Tab. S3**). The PCE of target device increase is 2.07% compared to the control

device. Meanwhile, as shown in supplementary **Fig. S10**, the highest PCE of the prepared 1cm^2 PSCs reaches 20.45% and the hysteresis of the HI is 0.013. Finally, the J-V diagram of the optimal device and in N_2 boxes at normal temperature after 15 days devices is shown in **Fig. 5d**. The device efficiency increased from 22.65% to 23.21% after 15 days of storage, with the largest change due to the increase in open circuit voltage from 1.14 V to 1.18 V, which may be caused by the presence of PbI_2 crystals in 2D/3D heterojunction. To verify the accuracy of our device test efficiency, we conducted external quantum efficiency (EQE) tests (**Fig. S11**) on the control and target devices. It was observed that the light absorption images of the target and the control device were essentially identical at various wavelengths. Additionally, the final integration current density indicated that there was not a significant difference in the current between the target device and the control device. However, the integration current density of the target device is 1.08 mAcm^{-2} higher than the J-V test current, and the integrated current density of the control device is 0.18 mAcm^{-2} higher than the J-V current. The error between the EQE Integrating current and the J-V current is less than 4%, which indicates that the J-V test current is consistent with the actual efficiency of PSCs. Then, we tested the dependence of the light intensity of the device, and the test results were shown in **Fig. 5e**. Meanwhile, the ideal factor obtained from the linear fitting of the test data for the final target device is 1.78, which is 0.67 lower than that of the control device. This indicates that the 2D/3D heterojunction perovskites exhibit lower non-radiative recombination and superior carrier transport capability. Under the same conditions, the 2D/3D heterojunction effectively inhibits carrier recombination in the target device. This is due to the interfacial passivation of 2D perovskite and PEABr on perovskite film, which reduces the surface defect density of perovskite. Moreover, this optimization improves the charge transport mechanics at the interface. To investigate the variation of defect density in perovskite films, as shown in **Fig. 5f**, the space charge-limited current (SCLC) measurements on PSCs electron-only devices are performed. The electron-only devices structure in the image is the device for our test of the SCLC. The defect density in perovskite films can be calculated by formula 3 based on the SCLC test results. Where V_{TFL} is the starting voltage of the trap filling limit, L

is the thickness of the active layer, ε is the relative perovskite dielectric constant, e is the basic charge and ε_0 is the vacuum dielectric constant. Then, the defect starting voltage of the control with the target PSCs is 0.55 V and 0.73 V. The decrease of the defect starting voltage means that the defect density of the device is lower, and it can also prove that the carrier recombination of the target device is suppressed.

$$N_t = \frac{2\varepsilon_0 \varepsilon V_{TFL}}{eL^2} \quad \text{(formula 3)}$$

The electrochemical impedance spectroscopy (EIS) test results are shown in **Fig. 5g**. In our device test, both the control and target devices showed a particularly small internal resistance R_0, the size of which is close to 0 Ω, so it is very small in the image, and there is basically no difference. However, the electrochemical impedance fitting radius of the 2D/3D heterojunction perovskite devices is larger than that of control devices. The increase in charge transfer resistance means that carrier transport of PSCs is more difficult. However, due to the presence of the 2D/3D heterojunction, the target perovskite film has better light absorption capacity, so the final device is more efficient. At the same time, as shown in **Fig. 5h**, to explore the differences in internal electric fields of the 2D/3D heterojunction devices with higher charge transfer resistance, the Mott-Schottky tests were carried out on the devices. The test results show that the internal electric field (V_{bi}) of the target device is 0.80 V and that of the control device is 0.77 V. The higher V_{bi} of the target device means that the driving force of charge separation is enhanced, which is conducive to carrier transport [38]. Finally, we placed the device in a completely dark environment to test the dark current of the device (shown in **Fig. 5i**). The results reveal that the dark current density of the control device is 1.03×10^{-1} mA/cm^2, whereas that of the target device is 6.41×10^{-4} mA/cm^2. The dark current of the target device is lower than that of the control device, suggesting that the incorporation of the 2D/3D heterojunction perovskite and the residual PEABr in the target device exerts a mitigating effect on the generation of leakage current.

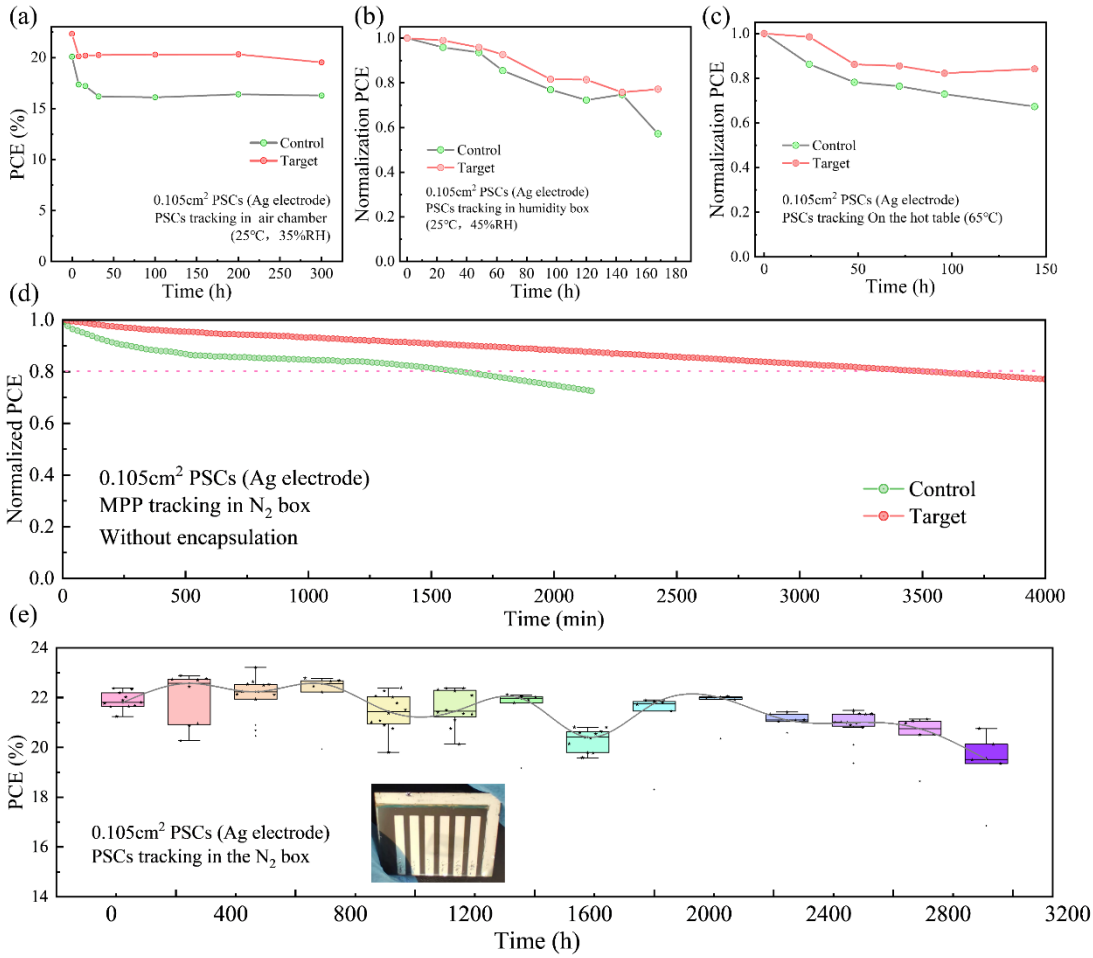

Figure 6. (a) Unpackaged devices are tested for stability when placed in air at 25℃ and 35%RH. (b) Unpackaged devices are placed in a constant humidity chamber at 25℃ and 45%RH for stability testing. (c) Stability testing of unpackaged devices on a hot table at 65℃. (d) MPP tracking test of unpackaged devices in the N_2 box. (e) Stability test of optimal device in normal temperature N_2 atmosphere.

The stability of PSCs is an important difficulty, so the stability test of the final device is an essential part. Next, the stability of the device is tested by the control device and the target device in various test environments. B. P. Kore et al studied three organic cations with different alkyl chain lengths, and used 2D perovskite as the encapsulation layer on top of 3D perovskite [39]. When the perovskite film is completely immersed in water, it can remain in water for 3 minutes, which means that the hydrophobicity of the perovskite film is significantly enhanced. Therefore, using 2D perovskite to improve the stability of the 3D perovskite is a promising method. Next, the stability of the target device and the control device will be tested. As shown in **Fig. 6a**, we placed the control

and the target device in the air (25℃, 35%RH), and the results showed that the stability of the target device was greatly improved compared with that of the control device. Upon storage in ambient air for a specified duration, the efficiency of the control device exhibited considerable variability, declining by 4% over the course of a single day. However, the target device efficiency experienced a mere 2% decrease, with any subsequent fluctuations being notably minimal. This stability improvement, we believe that 2D/3D perovskite and PEABr play an effective role in inhibiting the defects of the device. However, we did not observe a tendency of increase in the efficiency of the target device under these conditions, and we speculate that this is the 2D/3D heterojunction changes too quickly under the influence of humidity. As shown in **Fig. 6b**, the same batch of devices was placed in a constant humidity chamber at 45%RH, and the efficiency of the control devices decreased by 80% after 60 hours. Secondly, the same batch of devices is placed on a hot table at 65°C for a temperature stability test (**Fig. 6c**), and the device efficiency decreased significantly, possibly due to the oxidation of the Ag electrode. However, the stability of the target device was still higher than that of the control device. In various storage stability tests, the stability of the target device is stronger than that of the control device, which indicates that the interface action of the PEABr and 2D/3D perovskite pair is worthy of attention.

Finally, the maximum power point (MPP) tracking test on the PSCs with Ag electrode was conducted (**Fig. 6d**), and the test results indicated that the efficiency of the target device decreased to 80% after 3500 minutes of continuous testing. This was a particularly surprising result in MPP tests of PSCs using Ag electrodes. As shown in **Fig. 6e**, the optimal PSCs is stored in the N_2 box for stability testing. The results showed that the efficiency of the target PSCs continued to increase (from 22.65% to 23.21%) after 300 hours of storage, a phenomenon rarely observed in the study of inverted PSCs. Simultaneously, this phenomenon is observable due to the relatively slow degradation of the PSCs within the N_2 environment. Furthermore, the notable enhancement in initial stability of the 2D/3D heterojunction perovskite is closely linked to the evolution of the respective film structures. Notably, the device maintains 89% of its initial efficiency after 3000 hours in the N_2 box, marking exceptionally high stability data for PSCs

employing silver electrodes. Detailed test data is shown in supplementary **Tab. S4**. This test result shows that the change of PEABr and the 2D/3D heterojunction on the upper surface of perovskite is beneficial for the stability of the PSCs.

3.Conclusion

In our research, we discovered that in the 2D/3D heterojunction PSCs tends to degrade over time during the operation. Additionally, the organic spacer molecules (PEABr) within the 2D perovskite lattice are separated from the upper surface of the perovskite during its long-term operation. In this separation process, the PbI_2 crystals will appear on the upper surface of the 2D/3D heterojunction perovskite film, which improves the carrier transport capacity at the interface and reduces the non-radiative recombination at the interface. In addition, by using optical characterization such as TA and PL to analyse the evolution process of 2D/3D, the carrier dynamic behaviour relationship corresponding to the evolution process is obtained. The V_{OC} of the PSCs increased from 1.14 V to 1.18 V and the PCE increased to 23.21% after the PSCs placed in the N_2 box for 300 hours. Finally, the unpackaged devices maintained 89% of their initial performance for 3000 hours in a room temperature N_2 box. Our work provides insights into the evolution mechanism of the 2D/3D heterojunctions and has important implications for tuning the 2D/3D structures and improving PSCs performance and stability.

References

[1] Y. Liu, S. Yuan, H. Zheng, M. Wu, S. Zhang, J. Lan, W. Li, J. Fan, Structurally Dimensional Engineering in Perovskite Photovoltaics, Advanced Energy Materials 13 (2023) 2300188.

[2] E. Ruggeri, S.D. Stranks, E. Manidakis, C.C. Stoumpos, C. Katan, Halide Perovskites: Low Dimensions for Devices, ACS Energy Letters 4 (2019) 2902-2904.

[3] C. Zuo, L. Ding, Drop-Casting to Make Efficient Perovskite Solar Cells under High Humidity, Angewandte Chemie International Edition 60 (2021) 11242-11246.

[4] A. Kojima, K. Teshima, Y. Shirai, T. Miyasaka, Organometal Halide Perovskites as Visible-Light Sensitizers for Photovoltaic Cells, Journal of the American Chemical Society 131 (2009) 6050-6051.

[5] H. Chen, C. Liu, J. Xu, A. Maxwell, W. Zhou, Y. Yang, Q. Zhou, A.S.R. Bati, H. Wan, Z. Wang, L. Zeng, J. Wang, P. Serles, Y. Liu, S. Teale, Y. Liu, M.I.

Saidaminov, M. Li, N. Rolston, S. Hoogland, T. Filleter, M.G. Kanatzidis, B. Chen, Z. Ning, E.H. Sargent, Improved Charge Extraction in Inverted Perovskite Solar Cells with Dual-site-binding Ligands, Science 384 (2024) 189-193.

[6] S. Sidhik, Y. Wang, M. De Siena, R. Asadpour, A.J. Torma, T. Terlier, K. Ho, W. Li, A.B. Puthirath, X. Shuai, A. Agrawal, B. Traore, M. Jones, R. Giridharagopal, P.M. Ajayan, J. Strzalka, D.S. Ginger, C. Katan, M.A. Alam, J. Even, M.G. Kanatzidis, A.D. Mohite, Deterministic Fabrication of 3D/2D Perovskite Bilayer Stacks for Durable and Efficient Solar Cells, Science 377 (2022) 1425-1430.

[7] I. Metcalf, S. Sidhik, H. Zhang, A. Agrawal, J. Persaud, J. Hou, J. Even, A.D. Mohite, Synergy of 3D and 2D Perovskites for Durable, Efficient Solar Cells and Beyond, Chemical Reviews 123 (2023) 9565-9652.

[8] L. Luo, H. Zeng, Z. Wang, M. Li, S. You, B. Chen, A. Maxwell, Q. An, L. Cui, D. Luo, J. Hu, S. Li, X. Cai, W. Li, L. Li, R. Guo, R. Huang, W. Liang, Z.-H. Lu, L. Mai, Y. Rong, E.H. Sargent, X. Li, Stabilization of 3D/2D Perovskite Heterostructures Via Inhibition of Ion Diffusion by Cross-linked Polymers for Solar Cells with Improved Performance, Nature Energy 8 (2023) 294-303.

[9] A.R.b.M. Yusoff, M.K. Nazeeruddin, Low-Dimensional Perovskites: From Synthesis to Stability in Perovskite Solar Cells, Advanced Energy Materials 8 (2018) 1702073.

[10] J. Gu, X. Sun, P. F. Chan, X. Lu, P. Zeng, J. Gong, F. Li, M. Liu, Constructing Low-dimensional Perovskite Network to Assist Efficient and Stable Perovskite Solar Cells, Journal of Energy Chemistry, 96 (2024) 625-632.

[11] P. Chen, Y. Bai, S. Wang, M. Lyu, J.-H. Yun, L. Wang, In Situ Growth of 2D Perovskite Capping Layer for Stable and Efficient Perovskite Solar Cells, Advanced Functional Materials 28 (2018) 1706923.

[12] E.-B. Kim, M.S. Akhtar, H.-S. Shin, S. Ameen, M.K. Nazeeruddin, A Review on Two-dimensional (2D) and 2D-3D Multidimensional Perovskite Solar Cells: Perovskites Structures, Stability, and Photovoltaic Performances, Journal of Photochemistry and Photobiology C: Photochemistry Reviews 48 (2021) 100405.

[13] G. Uzurano, N. Kuwahara, T. Saito, K. Abe, S. Miyake, D. Hishida, Y. Takeoka, A. Fujii, M. Ozaki, 2D/3D Perovskite Heterostructure Solar Cell with Orientation-controlled Dion–Jacobson 2D Phase, Applied Physics Express 16 (2023) 041005.

[14] P. Li, Y. Zhang, C. Liang, G. Xing, X. Liu, F. Li, X. Liu, X. Hu, G. Shao, Y. Song, Phase Pure 2D Perovskite for High-Performance 2D–3D Heterostructured Perovskite Solar Cells, Advanced Materials 30 (2018) 1805323.

[15] C.W. Jang, H. Kim, M.K. Nazeeruddin, D.H. Shin, S.-H. Choi, Piezo-electric and -Phototronic Effects of Perovskite 2D/3D Heterostructures, Nano Energy 84 (2021) 105899.

[16] M.A. Mahmud, T. Duong, J. Peng, Y. Wu, H. Shen, D. Walter, H.T. Nguyen, N. Mozaffari, G.D. Tabi, K.R. Catchpole, K.J. Weber, T.P. White, Origin of Efficiency and Stability Enhancement in High-Performing Mixed Dimensional 2D-3D Perovskite Solar Cells: A Review, Advanced Functional Materials 32 (2022) 2009164.

[17] D. Gao, B. Li, Z. Li, X. Wu, S. Zhang, D. Zhao, X. Jiang, C. Zhang, Y. Wang, Z.

Li, N. Li, S. Xiao, W.C.H. Choy, A.K.Y. Jen, S. Yang, Z. Zhu, Highly Efficient Flexible Perovskite Solar Cells through Pentylammonium Acetate Modification with Certified Efficiency of 23.35%, Advanced Materials 35 (2023) 2206387.
[18] M. Xiong, W. Zou, K. Fan, C. Qin, S. Li, L. Fei, J. Jiang, H. Huang, L. Shen, F. Gao, A.K.Y. Jen, K. Yao, Tailoring Phase Purity in the 2D/3D Perovskite Heterostructures Using Lattice Mismatch, ACS Energy Letters 7 (2022) 550-559.
[19] X. Dong, Y. Tang, Y. Li, X. Li, Y. Zhao, W. Song, F. Wang, S. Xu, Y. Zhou, C. Ran, Z. Miao, L. Song, Z. Wu, Boosting MA-based Two-dimensional Ruddlesden-Popper perovskite Solar Cells by Incorporating A Binary Spacer, Journal of Energy Chemistry, 95 (2024) 348-356.
[20] C. Li, R. Zhu, Z. Yang, J. Lai, J. Tan, Y. Luo, S. Ye, Boosting Charge Transport in a 2D/3D Perovskite Heterostructure by Selecting an Ordered 2D Perovskite as the Passivator, Angewandte Chemie International Edition 62 (2023) e202214208.
[21] P. Sebastia-Luna, U. Pokharel, B.A.H. Huisman, L.J.A. Koster, F. Palazon, H.J. Bolink, Vacuum-Deposited Cesium Tin Iodide Thin Films with Tunable Thermoelectric Properties, ACS Applied Energy Materials 5 (2022) 10216-10223.
[22] J. Qian, J. He, Q. Zhang, C. Zhu, S. Chen, Z. Wei, X. Leng, Z. Zhou, B. Shen, Y. Peng, Q. Niu, S. Yang, Y. Hou, Minimizing Interfacial Energy Losses in Inverted Perovskite Solar Cells by A Dipolar Stereochemical 2D Perovskite Interface, Journal of Energy Chemistry, 90 (2024) 496-503.
[23] J. Duan, Y. Zhao, B. He, Q. Tang, High-Purity Inorganic Perovskite Films for Solar Cells with 9.72 % Efficiency, Angewandte Chemie International Edition 57 (2018) 3787-3791.
[24] T. Niu, Y.-M. Xie, Q. Xue, S. Xun, Q. Yao, F. Zhen, W. Yan, H. Li, J.-L. Brédas, H.-L. Yip, Y. Cao, Spacer Engineering of Diammonium-Based 2D Perovskites toward Efficient and Stable 2D/3D Heterostructure Perovskite Solar Cells, Advanced Energy Materials 12 (2022) 2102973.
[25] B.R. Wygant, A.Z. Ye, A. Dolocan, Q. Vu, D.M. Abbot, C.B. Mullins, Probing the Degradation Chemistry and Enhanced Stability of 2D Organolead Halide Perovskites, Journal of the American Chemical Society 141 (2019) 18170-18181.
[26] L. Gao, P. Hu, S. Liu, Low-dimensional Perovskite Modified 3D Structures for Higher-performance Solar Cells, Journal of Energy Chemistry, 81(2023) 389-403.
[27] A.A. Sutanto, R. Szostak, N. Drigo, V.I.E. Queloz, P.E. Marchezi, J.C. Germino, H.C.N. Tolentino, M.K. Nazeeruddin, A.F. Nogueira, G. Grancini, In Situ Analysis Reveals the Role of 2D Perovskite in Preventing Thermal-Induced Degradation in 2D/3D Perovskite Interfaces, Nano Letters 20 (2020) 3992-3998.
[28] X. Zhang, W. Zhou, X. Chen, Y. Chen, X. Li, M. Wang, Y. Zhou, H. Yan, Z. Zheng, Y. Zhang, Dual Optimization of Bulk and Surface via Guanidine Halide for Efficient and Stable 2D/3D Hybrid Perovskite Solar Cells, Advanced Energy Materials 12 (2022) 2201105.
[29] W. Zhou, L. Jia, M. Chen, X. Li, Z. Su, Y. Shang, X. Jiang, X. Gao, T. Chen, M. Wang, Z. Zhu, Y. Lu, S. Yang, An Improbable Amino-Functionalized Fullerene Spacer Enables 2D/3D Hybrid Perovskite with Enhanced Electron Transport in Solar Cells, Advanced Functional Materials 32 (2022) 2201374.

[30] H. Li, C. Zhang, C. Gong, D. Zhang, H. Zhang, Q. Zhuang, X. Yu, S. Gong, X. Chen, J. Yang, X. Li, R. Li, J. Li, J. Zhou, H. Yang, Q. Lin, J. Chu, M. Grätzel, J. Chen, Z. Zang, 2D/3D Heterojunction Engineering at the Buried Interface Towards High-Performance Inverted Methylammonium-free Perovskite Solar Cells, Nature Energy 8 (2023) 946-955.

[31] R. Azmi, E. Ugur, A. Seitkhan, F. Aljamaan, A.S. Subbiah, J. Liu, G.T. Harrison, M.I. Nugraha, M.K. Eswaran, M. Babics, Y. Chen, F. Xu, T.G. Allen, A.u. Rehman, C.-L. Wang, T.D. Anthopoulos, U. Schwingenschlögl, M. De Bastiani, E. Aydin, S. De Wolf, Damp Heat–stable Perovskite Solar Cells with Tailored-dimensionality 2D/3D Heterojunctions, Science 376 (2022) 73-77.

[32] Y. Bai, Z. Huang, X. Zhang, J. Lu, X. Niu, Z. He, C. Zhu, M. Xiao, Q. Song, X. Wei, C. Wang, Z. Cui, J. Dou, Y. Chen, F. Pei, H. Zai, W. Wang, T. Song, P. An, J. Zhang, J. Dong, Y. Li, J. Shi, H. Jin, P. Chen, Y. Sun, Y. Li, H. Chen, Z. Wei, H. Zhou, Q. Chen, Initializing Film Homogeneity to Retard Phase Segregation for Stable Perovskite Solar Cells, Science 378 (2022) 747-754.

[33] X. Liu, D. Luo, Z.-H. Lu, J.S. Yun, M. Saliba, S.I. Seok, W. Zhang, Stabilization of Photoactive Phases for Perovskite Photovoltaics, Nature Reviews Chemistry 7 (2023) 462-479.

[34] S. Masi, A.F. Gualdrón-Reyes, I. Mora-Seró, Stabilization of Black Perovskite Phase in $FAPbI_3$ and $CsPbI_3$, ACS Energy Letters 5 (2020) 1974-1985.

[35] T. Mahmoudi, Y. Wang, Y.-B. Hahn, Stability Enhancement in Perovskite Solar Cells with Perovskite/Silver–Graphene Composites in the Active Layer, ACS Energy Letters 4 (2019) 235-241.

[36] Z. Yang, B. Cai, B. Zhou, T. Yao, W. Yu, S. Liu, W.-H. Zhang, C. Li, An Up-scalable Approach to $CH_3NH_3PbI_3$ Compact Films for High-Performance Perovskite Solar Cells, Nano Energy 15 (2015) 670-678.

[37] Y. Lei, Y. Zhang, J. Huo, F. Ding, Y. Yan, Y. Shen, X. Li, W. Kang, Z. Yan, Stability Strategies and Applications of Iodide Perovskites, Small (2024) 2311880.

[38] Z. Huang, Z. Ma, C. Deng, T. Yu, G. Li, Z. Du, W. You, J. Yang, Y. Chen, Y. Li, S. Hou, Q. Yang, Q. Zhang, H. Du, Y. Li, H. Shu, Q. Liu, C. Peng, Y. Huang, J. Yu, Y. Lin, K. Sun, W. Long, Aging-Resistant Precursor with Ultrawide Annealing Window for 24.08% Perovskite Solar Cells, Advanced Energy Materials 14 (2024) 2302769.

[39] J. Zhang, S. Langner, J. Wu, C. Kupfer, L. Lüer, W. Meng, B. Zhao, C. Liu, M. Daum, A. Osvet, N. Li, M. Halik, T. Stubhan, Y. Zhao, J.A. Hauch, C.J. Brabec, Intercalating-Organic-Cation-Induced Stability Bowing in Quasi-2D Metal-Halide Perovskites, ACS Energy Letters 7 (2022) 70-77.

[40] P. Li, Y. Zhang, C. Liang, G. Xing, X. Liu, F. Li, X. Liu, X. Hu, G. Shao, Y. Song, Phase Pure 2D Perovskite for High-Performance 2D/3D Heterostructured Perovskite Solar Cells, Advanced Materials 30 (2018) 1805323.

[41] Y. Lv, D. Si, X. Song, K. Wang, S. Wang, Z. Zhao, C. Hao, L. Wei, Y. Shi, Pseudohalogen-Based 2D Perovskite: A More Complex Thermal Degradation Mechanism Than 3D Perovskite, Inorganic Chemistry 57 (2018) 2045-2050.

[42] Z. Wang, Q. Ou, Y. Zhang, Q. Zhang, H.Y. Hoh, Q. Bao, Degradation of Two-

Dimensional $CH_3NH_3PbI_3$ Perovskite and $CH_3NH_3PbI_3$/Graphene Heterostructure, ACS Applied Materials & Interfaces 10 (2018) 24258-24265.
[43] Q. Liu, Z. Ma, Y. Li, G. Yan, D. Huang, S. Hou, W. Zhou, X. Wang, J. Ren, Y. Xiang, R. Ding, X. Yue, Z. Du, M. Zhang, W. Zhang, L. Duan, Y. Huang, Y. Mai, Heterogeneous Lead Iodide Obtains Perovskite Solar Cells with Efficiency of 24.27%, Chemical Engineering Journal 448 (2022) 137676.
[44] Y. Liu, H. Zhou, Y. Ni, J. Guo, R. Lu, C. Li, X. Guo, Revealing Stability Origin of Dion-Jacobson 2D Perovskites with Different-Rigidity Organic Cations, Joule 7 (2023) 1016-1032.
[45] Y. Zhong, G. Liu, Y. Su, W. Sheng, L. Gong, J. Zhang, L. Tan, Y. Chen, Diammonium Molecular Configuration-Induced Regulation of Crystal Orientation and Carrier Dynamics for Highly Efficient and Stable 2D/3D Perovskite Solar Cells, Angewandte Chemie International Edition 61 (2022) e202114588.
[46] G. Grancini, C. Roldán-Carmona, I. Zimmermann, E. Mosconi, X. Lee, D. Martineau, S. Narbey, F. Oswald, F. De Angelis, M. Graetzel, M.K. Nazeeruddin, One-Year Stable Perovskite Solar Cells by 2D/3D Interface Engineering, Nature Communications 8 (2017) 15684.
[47] X. Jiang, J. Zhang, S. Ahmad, D. Tu, X. Liu, G. Jia, X. Guo, C. Li, Dion-Jacobson 2D-3D Perovskite Solar Cells with Improved Efficiency and Stability, Nano Energy 75 (2020) 104892.
[48] F. Wang, X. Jiang, H. Chen, Y. Shang, H. Liu, J. Wei, W. Zhou, H. He, W. Liu, Z. Ning, 2D-Quasi-2D-3D Hierarchy Structure for Tin Perovskite Solar Cells with Enhanced Efficiency and Stability, Joule 2 (2018) 2732-2743.
[49] Q. Lai, R. Zhuang, K. Zhang, T. Wu, L. Xie, R. Zhao, L. Yang, Y. Wang, Y. Hua, A Multifunctional Liquid Crystal as Hole Transport Layer Additive Enhances Efficiency and Stability of Perovskite Solar Cells, Angewandte Chemie International Edition, 62 (2023) e202305670.
[50] A.D. Wright, C. Verdi, R.L. Milot, G.E. Eperon, M.A. Pérez-Osorio, H.J. Snaith, F. Giustino, M.B. Johnston, L.M. Herz, Electron-Phonon Coupling in Hybrid Lead Halide Perovskites, Nature Communications 7 (2016) 11755.

2D/3D Heterojunction Carrier Dynamics and Interface Evolution for Efficient Inverted Perovskite Solar Cells

Yi Chen[1], Zhu Ma[1], Zhuowei Du[1], Wei You[1], Junbo Yang[1], Qiang Yang[1], Qian Zhang[1], Hao Du[1], Yixian Li[1], Fuchun Gou[1], Shanyue Hou[1], Shenshen Zheng[1], Fengying Zhang[1], Cheng Huang[1], Yuelong Huang[1], Yan Xiang[1]*, Liming Ding[2]*, Kuan Sun[3]*, Mojtaba Abdi-Jalebi[4]**

1. School of New Energy and Materials, Southwest Petroleum University (SWPU), Chengdu 610500, China

2. Center for Excellence in Nanoscience, Key Laboratory of Nanosystem and Hierarchical Fabrication (CAS), National Center for Nanoscience and Technology, Beijing 100190, China

3. Key Laboratory of Low-grade Energy Utilization Technologies and Systems (MoE), School of Energy and Power Engineering, Chongqing University, Chongqing 400044, China

4. Institute for Materials Discovery University College London Malet Place, London WC1E 7JE, UK

Corresponding Author

E-mail:deve198509@163.com (Z. Ma), xiangyan0718@163.com (Y. Xiang)

ding@nanoctr.cn (L. Ding), kuan.sun@cqu.edu.cn (K. Sun),

m.jalebi@ucl.ac.uk (M. Abdi-Jalebi)

Abstract

The 2D/3D heterojunction perovskites have garnered increasing attention due to their exceptional moisture and thermal stability. However, few works have paid attention to the influence of the subsequent change process of 2D/3D heterojunction PSC on the stability of PSCs. Moreover, the evolution of the interface and carrier dynamic behavior of the 2D/3D perovskite films with long-term operation has not been systematically developed before. In this work, the effects of 2D/3D heterojunction evolution on the interface of perovskite films and different carrier dynamics during 2D/3D evolution are systematically analyzed for the first time. The decomposition of 2D/3D heterojunction in the perovskite film will have a certain impact on the surface and carrier dynamics behavior of perovskite. During the evolution of 2D/3D heterojunction, PbI_2 crystals will appear, which will improve the interfacial energy level matching between the electron transport layer and perovskite film. With a long evolution time, some holes will appear on the surface of perovskite film. The open circuit voltage (V_{OC}) of PSCs increased from 1.14 V to 1.18 V and the PCE increased to 23.21% after 300 hours storage in the nitrogen atmosphere, and maintained 89% initial performance for with 3000 hours stability test in N_2 box. This discovery has a significant role in promoting the development of inverted heterojunction PSCs and constructing the revolution mechanism of charge carrier dynamic.

Keywords: 2D/3D heterojunction, interface, carrier dynamics, evolution, inverted PSCs.

1. Introduction

The organic-inorganic hybrid halogenated perovskites have attracted much attention due to their favorable photoelectric properties [1-3], and the PCE of perovskite solar cells (PSCs) has risen rapidly from 3.8% [4] in 2009 to exceeding 26% [5] in 2024. Unfortunately, the three-dimensional (3D) is not stable enough due to its own ion migration and phase transitions, which seriously hinders the commercialization of PSCs [6-8]. The two-dimensional (2D) perovskites are stable enough, but the PCE is not that high due to their poor carrier transport ability. Compared with 3D perovskites and 2D perovskites, the 2D/3D heterojunction perovskites have been widely concerned for their good stability and excellent photoelectric properties [9-15].

In the past decade, 2D/3D heterojunction PSCs have undergone significant development [16,17] and various preparation methods of 2D/3D heterojunction perovskite have been proposed, such as bulk phase doping [18,19], surface treatment [20] and vapor deposition [21] methods. One of the most promising ways to constructing 2D/3D heterojunction is spin-coating organic spacer molecules on top of 3D perovskite film [22,23]. Meanwhile, the residual organic spacers will affect the electronic properties of 2D/3D heterojunction interface [24]. Furthermore, the presence of 2D/3D heterojunctions can also suppress the degradation of 3D perovskite crystals in air environmental conditions [25]. When the perovskite film is affected by both water and heat, the water molecules can only penetrate 3D perovskite film after the 2D perovskite layer disappears, which resulting in the degradation and phase transition of 3D perovskite [26]. At the same time, in situ X-ray scattering experiments at the 2D/3D interface, 3D perovskite crystals dynamically transformed into 2D/3D mixed phases and hindered the degradation of 3D perovskite to PbI_2 [27]. Therefore, constructing 2D/3D heterojunctions in perovskites can effectively improves the crystallization of 3D perovskites by adding 2D perovskites [28], enhances carrier transport ability by constructing 2D passivation layer on the upper interface of 3D perovskites [29], improves charge extraction efficiency and reduces non-radiative recombination by constructing 2D perovskites on the bottom interface of 3D perovskites [30,31]. Although 2D/3D

heterostructure synthesizes the performance advantages of both sides, the degradation and transition mechanisms of 2D and 3D are different, which will inevitably affect the photoelectric conversion performance of PSCs.

3D perovskites are susceptible to phase transitions and degradation caused by moisture, light, and temperature in the environment due to its special crystal structure [32]. In the phase structure of 3D perovskites, the black alpha phase perovskites exhibit strong light absorption capacity, while the yellow delta phase perovskites exhibit poor photovoltaic effect [33]. At the same time, the alpha phase of 3D perovskite spontaneously transitions to the delta phase because of ion migration within the perovskite crystal, the accumulation of defect states, and the rotation and tilt of the lead iodide octahedron [PbI_6] [34]. When perovskite is placed under long-term light, perovskite will destroy the cubic phase crystal due to its own ion migration. In addition, perovskite is sensitive to humidity, and hydrolysis reaction is easy to occur in high humidity environment [35,36]. The long-term heating can also lead to the degradation of perovskite, because heating will produce some active substances to destroy the original stable cubic structure of perovskite [37,38]. Meanwhile, the 2D perovskites consist of alternating layers of organic cation spacers and inorganic frames [39]. Compared to 3D perovskites, the 2D perovskites can exhibit more stable performance in humidity and moisture environments because their layered structure reduces the penetration and influence of water molecules [40]. However, even though 2D perovskites are more stable in high humidity and moisture environments, hydrolysis reactions can still occur in extremely humid environments [33]. In long-term thermal stability tests, the 2D perovskites also showed excellent performance compared to 3D perovskites, but the 2D perovskites still degrade at higher temperatures due to thermal stress [41]. Among them, the degradation of 2D perovskite is mainly caused by cationic evaporation under the action of thermal stress [42,43]. In addition, the rigidity and heat resistance of organic spacer molecules used to construct 2D perovskites will also affect the stability and thermal decomposition ability of 2D perovskites [44]. In the process of long-term stable operation of perovskite, 3D perovskite and 2D perovskite crystals will degrade due to the influence of external environmental factors, thereby reducing the photoelectric

capacity of perovskite. However, there are few studies on the subsequent evolution process of 2D/3D heterojunction interfaces and charge carrier dynamic behavior with the evolution of 2D/3D heterojunction perovskite [45]. In addition, many studies have shown that the stability of perovskite solar cells built with 2D/3D heterogeneous structures has been greatly improved [46], and the final stability improvement of PSCs is due to the existence of 2D perovskite, which inhibits the interface defects [47,48]. However, few people pay attention to the influence of the subsequent change process of 2D/3D heterojunction PSC on the stability of PSCs. A better understanding of the carrier dynamics of this evolution is of great significance for the development of 2D/3D heterojunctions.

In this work, the 2D/3D heterojunction perovskite films were placed on the heating table at 60℃ to accelerate the evolution process. With time going, a series of changes will occur on the surface of 2D/3D perovskite films, and it is easier to find the changes of 2D decomposed surface morphology and carrier dynamics. By studying the changes of 2D/3D perovskite interface, we can more clearly understand the effects of 2D/3D heterojunction evolution behavior. Finally, the dynamic behavior of 2D/3D perovskite films during evolution is compared. The surface variation and carrier dynamics of perovskite thin films are important factors affecting the stability of PSCs.

2. Test results and analysis

2.1 Evolution of perovskite films

In this experiment, the one-step reverse-solvent engineering was used to fabricate inverted perovskite solar cells (PSCs) initially. Firstly, as illustrated in Fi**g. S1**, the electrostatic potential of PEABr molecular structure is analysed by using the Gaussian view in an ideal state without considering the influence of other external factors. The results show that the Br^- containing end exhibits a notably intense signal of negative charge region signal, suggesting that the Br^- containing branch chain has a stronger attraction towards positively charged ions within PEABr molecules. However, the benzene ring shows positive charge accumulation, and the nitrogen atom in the side chain shows stronger positive charge accumulation. This indicates that both the benzene

ring and the nitrogen atom have a stronger binding affinity for negatively charged ions.

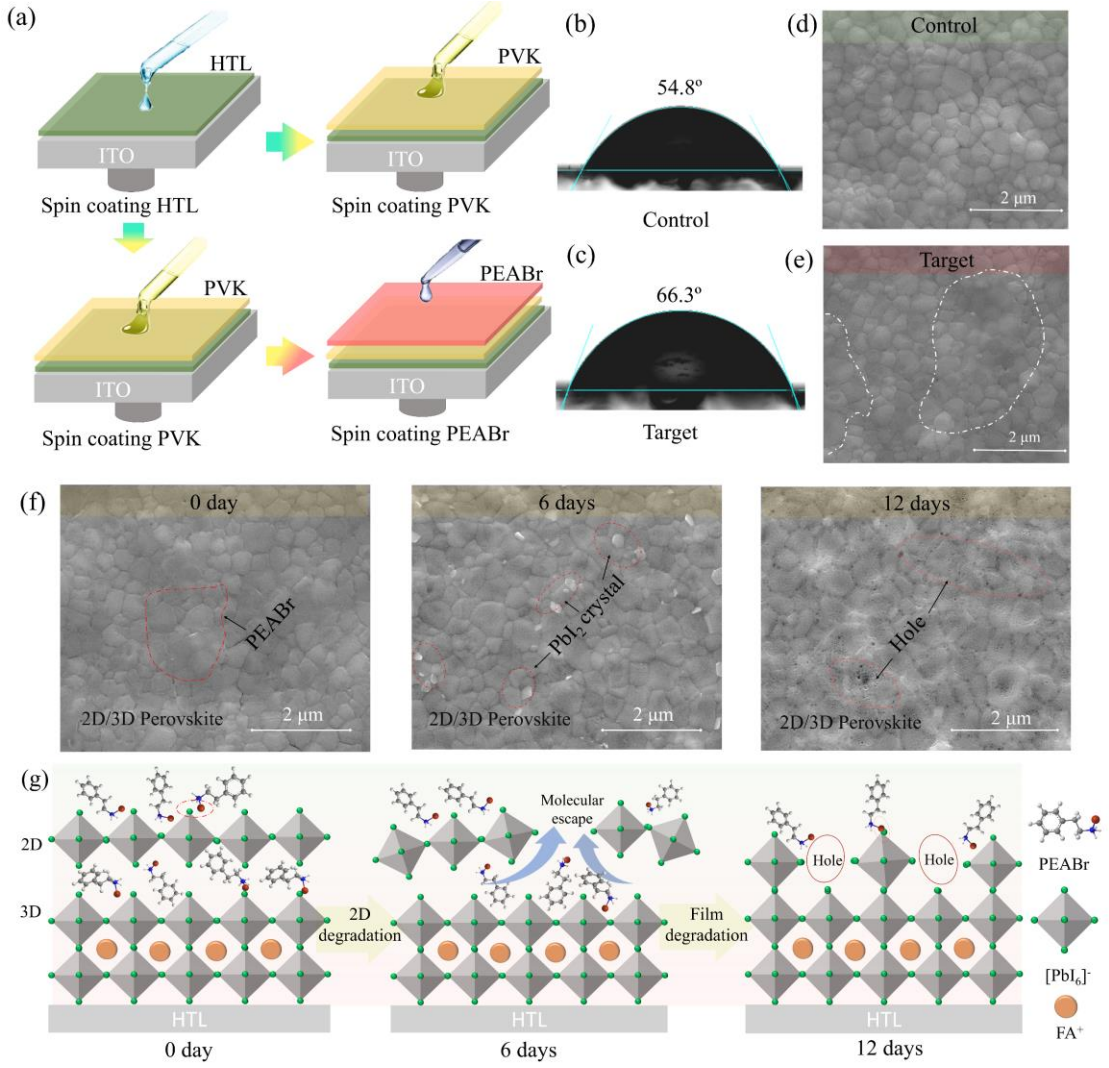

Figure 1. (a) Schematic diagram of perovskite film construction by different method. (b) Contact angle test diagram of perovskite film of control. (c) Contact angle test diagram of perovskite film of control target. (d) SEM image of perovskite film of control. (e) SEM image of perovskite film of target. (f) Surface diagram of perovskite films with target film placed on a hot table at 60℃ for different storage times. (g) schematic diagram of the 2D/3D interface change process of target perovskite film on the hot table at 60℃ for different time.

As shown in **Fig. 1a**, this is the process of experimentally constructing the 2D/3D heterojunction by spinning a layer of PEABr on the upper surface of 3D perovskite. This organic cation on the upper surface of the 3D perovskite will cause the 3D perovskite to be transformed into a low-dimensional perovskite. In the figure, films that are not coated with PEABr are labeled as the control, while the films coated with PEABr

are labeled as the target. In the process of constructing the 2D/3D heterojunction, compared with the control film, there is a special phenomenon after the PEABr spin coating on the upper surface of the perovskite film, which showed a colored halo of the perovskite film. Then, the contact angle test was conducted on the perovskite film to explore the impact of 2D/3D heterostructures and residual PEABr on the upper surface of both the control perovskite and the target perovskite films on the subsequent spin coating process. It can be seen from **Fig. 1d** and **1e** that the contact angle of the control perovskite film is 54.8°, while the target perovskite film is 66.3°. The water contact angle of the 2D/3D heterojunction after being constructed with PEABr shows an improvement of 11.5°. This indicates that the residual PEABr and the 2D/3D heterojunction on the upper surface of 3D perovskite improved the hydrophobicity of the film and adjusted the interface morphology of the film. At the same time, a humidity stability test of the perovskite film was conducted at 25℃ and 45%RH (**Fig. S2**). The results indicated that the surfaces of both the target film and the control perovskite film did not exhibit significant changes after 1000 hours of storage. However, in comparison to the control perovskite film, the colour of the edge of the target perovskite film has changed significantly, which we believe is caused by the residual PEABr on the surface of the perovskite. The scanning electron microscopy (SEM) test results, as shown in **Fig. 1d and 1e**, reveal that the grain size of both the target and control perovskite films was similar. However, there were significant gaps between the grains in the control film, making it easier for PEABr to react with the 3D perovskite. Moreover, these voids will also cause PEABr molecules to gather around them. It can be clearly seen in the test results that there are some residual PEABr molecules in the target perovskite film grain gaps. At the same time, the SEM test results of various scales and positions of perovskite films in **Fig. S3** indicate that this phenomenon is not unique. This phenomenon also demonstrates that the surface adhesion of residual PEABr molecules on 2D/3D perovskite plays a role in passivating interface defects, as characterized through further analysis. Then, as shown in **Fig. S4**, to investigate the thermal stability of the perovskite films, both the control and target perovskite films were subjected to continuous heating on a hot plate at 60℃. It can be observed that the perovskite in the

control film has essentially decomposed after 1400 hours, whereas the target film shows a certain black phase after the same duration, indicating greater stability in the target perovskite film. In addition, an unidentified substance precipitated on the upper surface of the target perovskite film after 300 hours. The presence of this unidentified substance suggests that the 2D/3D heterojunction of perovskite has changed during long-term stable operation, which may be caused by the decomposition of the 2D perovskite and the residue of PEABr molecules on the surface of perovskite. This phenomenon offers an opportunity to investigate the evolutionary mechanisms of the 2D/3D heterostructure perovskite films during extended operational periods. Therefore, we can summarize an evolutionary mechanism by conducting tests and characterizations on the 2D/3D heterostructure perovskite films with varying annealing durations.

As shown in **Fig. 1f**, the residual PEABr molecules exist on the upper surface of the fresh (0 day) perovskite film. From the top view of the perovskite film, there are some incomplete substances in the grain gap of perovskite. Moreover, after the same piece of perovskite film was placed on the heating platform for 6 days, some white bright parts appeared in the top view of the SEM, which was proved to be PbI_2 in the previous literature. With the increase of time, the PbI_2 disappeared in the SEM top view of the target perovskite film after 12 days annealing. The lead iodide present during the decomposition of the 2D perovskite may interact with the original FA^+ and PEA^+ ions. At the same time, it can be clearly found that more tiny holes appear on the upper surface of the perovskite film after 12 days of placement, and the grain size of the perovskite film hardly changes during the placement process, which means that the evolution process of the 2D/3D perovskite is beneficial to the crystal stability of the 3D perovskite. Through subsequent characterization tests, a structural evolution process of the upper surface of perovskite films was proposed (**Fig. 1g**). After the target perovskite film is left for 6 days, the 2D perovskite within the 2D/3D heterojunction film will gradually transform. The lead iodide will start to appear on the surface of the film, and PEABr molecules from inside the perovskite will migrate to the surface as the annealing process continues. Over time, the lead iodide appearing on the surface of the perovskite film is covered by the PEABr molecules or reacts with the 3D perovskite at the bottom,

and the PEABr molecules appearing on the upper interface of the perovskite will continue to play an interface passivation effect on the interface of the perovskite. This corresponds to the stability test results in the following section.

2.2 Evolution of perovskite carrier dynamics

The study of carrier transfer kinetics in 2D/3D perovskite films using femtosecond transient absorption spectroscopy (fs-TA) is crucial for comprehending enhancements in their photoelectric properties. **Fig. 2a-2c** and **Fig. S5a** are two-dimensional false-color images of perovskite film on quartz glass substrate with laser excitation of 700 nm, pump flow of 5 $\mu J \cdot cm^{-2}$, and carrier density of 1.34×10^{17} cm^{-3}. The spectra of the four samples show a ground-state bleaching (GSB) centered at 1.58 eV. This bleaching feature indicates that the carrier in the perovskite film transitions from the ground state to the excited state under laser excitation, causing the light absorption difference ΔA to change significantly on a ps scale due to the pumping process. As shown in **Fig. 2a–2c**, it can be found that the duration of bleaching region of the 2D/3D heterostructure perovskite films does not change significantly. Moreover, the variation range of the light absorption difference ΔA of the samples at different placement times is small, and it also indicates that the decomposition of 2D/3D heterojunction has a certain protective effect on 3D perovskite. The **Fig. 2d-2f** and **Fig. S5b** show the normalized time spectra of the control and target perovskite films in the time delay range of 0.4 ps to 10 ps. We found that both the control and the 2D/3D heterojunction perovskite film have a distinct 750-800 nm high-energy tail region (marked in blue) in the TA spectrum, which also reflects the cooling process of the hot carrier. It is noteworthy that the high-energy tail shrinkage rate of 2D/3D heterojunction perovskite films is faster than that of control films, which indicates that 2D/3D heterojunction changes the carrier cooling dynamics in perovskite films.

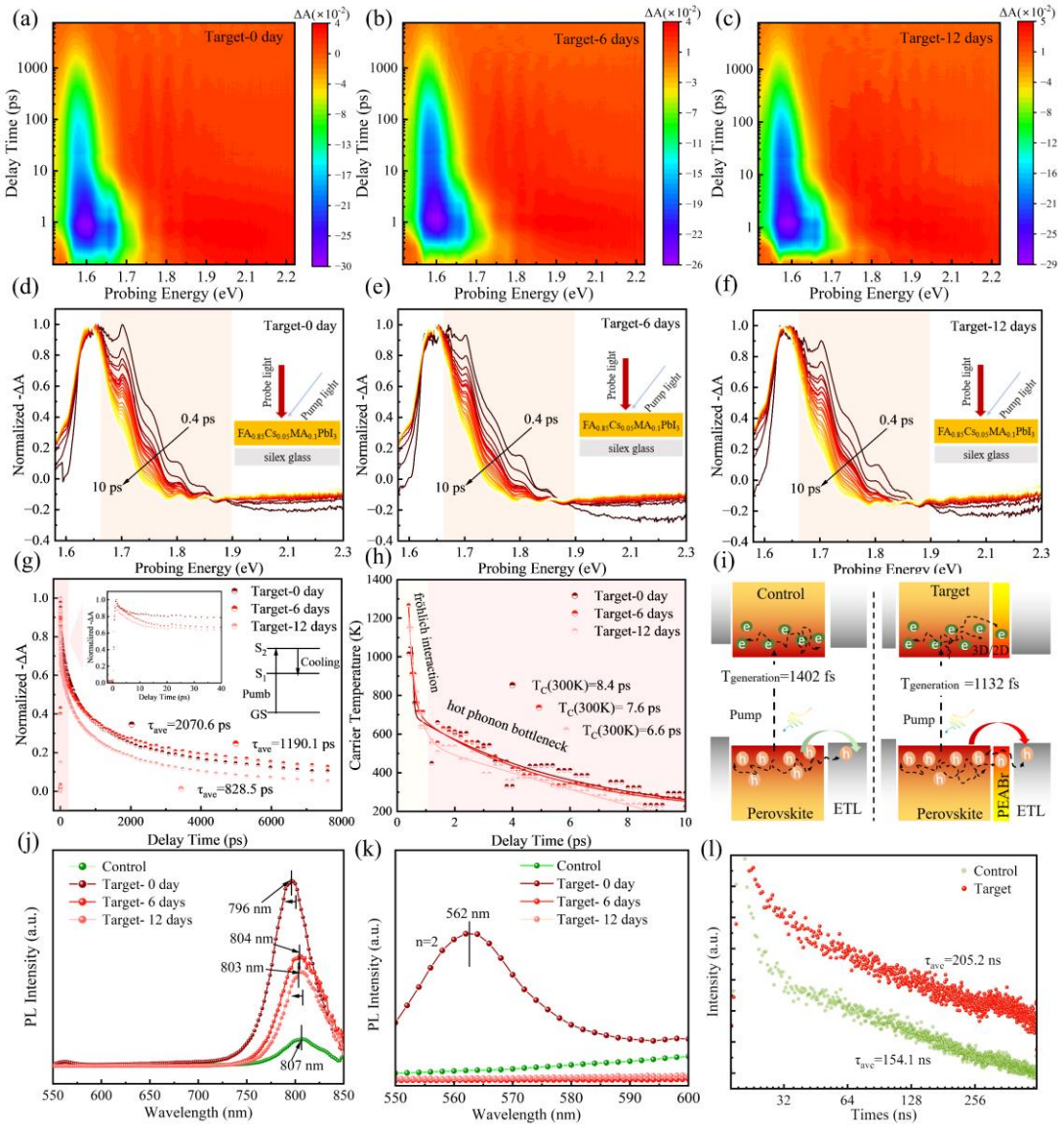

Figure 2. Fs-TA measurements of the 2D/3D perovskite films. (a-c) Two-dimensional false-color image of TA spectral perovskite film on a hot table at 60℃ for different time. (d-f) The TA spectra recorded at several delay times from 0.4 to 10 ps. (g) The corresponding normalized attenuation kinetics curve at 788 nm. (h) Hot carrier cooling time curve of target perovskite film. (i) The interface is between the schematic diagram of electron generation and extraction HTL and Perovskite. (j) PL spectra of control and target perovskite films with different storage times on 60℃ hot table. (k) PL spectra of control and target perovskite films with 550-600 nm wavelength. (l) TRPL spectrum of perovskite films with ITO substrate.

Fig. 2g and **Fig. S5c** show the carrier dynamics curves of perovskite thin films obtained from the highest point of excitation signal. The fitting results obtained by the three-exponential function fitting method on the data in the figure are shown in **Tab.**

S1. At a delay time of 1 ns, the normalized decay rate (ΔA) of the initial 2D/3D perovskite was only 65.17%, while the control perovskite film reached 72.38%. The ΔA of target-6 days perovskite is only 64.38%, compared to 73.61% for target-12 days perovskite films. 2D/3D perovskite films show a higher charge density and slower decay rate. In addition, TA decay can be well fitted using a three-exponential fitting model, and the corresponding parameters are listed in **Tab. S1**. Compared to a pure 3D perovskite with a charge recomposite life of 840.8 ps, the 2D/3D perovskite has a longer life, with a target-0 day of 2070.6 ps, target-6 days of 1190.1 ps, and target-12 days of 828.5 ps. The carrier lifetime of 2D/3D perovskites is longer, indicating that 2D perovskites can reduce the density of defect states and effectively manipulate carrier transfer. At the same time, the evolution process of 2D/3D also influences the defect state and charge transport of perovskite. In the range of 0-1ps, the excitation process of perovskite thin film is displayed, and the target is almost the same as that of perovskite thin film, and the target is almost the same as that of controlling the excitation strength of perovskite thin film. However, it can be clearly seen that the carrier dynamics of the target device changes more slowly during the subsequent carrier cooling process. This means that the carrier lifetime and carrier transport behavior change. Moreover, these high-energy tails gradually disappear from 0.4 ps to 10 ps, suggesting that the hot carrier cooling process in these samples can be evaluated by a hot carrier temperature (Tc) higher than the perovskite lattice temperature. By fitting the high-energy region (red background region) of the above fs-TA spectrum with the following Maxwell-Boltzmann distribution function (formula 1 and 2), the relationship between the hot carrier cooling time and the contraction rate of the high-energy tail can be obtained [49]:

$$\Delta T(\mathrm{h}\omega) = -T_0 exp\left(\frac{E_F - h\omega}{k_B T_c}\right) \quad \text{(formula 1)}$$

$$\Delta A = -log\left(1 + \frac{\Delta T}{T}\right) \quad \text{(formula 2)}$$

where E_F is the Fermi level, ΔT is the amplitude of bleaching at a specific detection wavelength, ΔA is the difference in light absorption at a specific detection wavelength, and k_B is the Boltzmann constant. The initial temperature of the hot carrier depends on the photoexcitation energy, which can be found in some previous studies [49]. Since the

wavelength and energy of the initial excitation laser are fixed, the relationship between the temperature of 2D/3D heterojunction perovskite hot carrier and the delay time can be determined by formulas 1 and 2. **Fig. 2h** and **Fig. S5d** show the change curve of carrier temperature (T_C) with delay time for perovskite films without and with 2D/3D heterojunction. The initial T_C of the control perovskite film is about 1511 K, and the initial T_C of 2D/3D perovskite film is about 1016 K, indicating that 2D perovskite can change the T_C cooling kinetics of 3D perovskite film. The initial T_C of 2D/3D perovskite film placed on a 60℃ hot table for 6 days is about 1266 K, and the initial T_C of 2D/3D perovskite film placed on a 60℃ hot table for 12 days is about 1147 K. All four perovskite films exhibit significant Tc decline, which is due to the ultrafast energy loss of perovskite films through the e carrier-LO-phonon scattering process on several ps time scales. The hot carrier motion behavior of perovskite thin films on the 1 ps time scale corresponds to fast carrier cooling via Fröhlich interaction [50]. The decrease in the thermal carrier temperature relaxation rate represented by another slow cooling process (1-10 ps) after the initial 1 ps attenuates is due to the hot phonon bottleneck effect. The carrier temperature of the 2D-free perovskite film attenuates from 1511 K to 1043 K over a 1 ps time scale, and does not attenuate to 300 K until 8 ps. The carrier temperature of the initial 2D/3D perovskite film attenuate from 1016 K to 639 K on a 1 ps time scale, and does not attenuate to 300 K until 8.4 ps. The 6 days 2D/3D perovskite film attenuates carrier temperatures from 1266 K to 634 K on a 1 ps time scale, and does not attenuate to 300 K until 7.6 ps. The 12 days 2D/3D perovskite film's carrier temperature attenuate from 1147k to 640 K on a 1 ps time scale, and does not attenuate to 300 K until 6.6 ps. Therefore, it can be concluded that the hot carrier cooling of 2D/3D heterojunction perovskite films requires more time, and the increase of hot carrier cooling time indicates that the carriers inside 2D/3D heterojunction perovskite have less energy loss during transport. Compared with the initial 2D/3D perovskite film, the hot carrier cooling time of the perovskite film placed for 6 days is longer, but the hot carrier cooling time of the perovskite film placed for 12 days is only 6.6 ps. Therefore, it can be concluded that more time is required for hot carrier cooling of the 2D/3D heterojunction films, and the increase in hot carrier cooling time indicates

that the carriers inside 2D/3D heterojunction perovskites have less energy loss during transport. **Fig. 2i** shows the excitation time diagram of perovskite film. The photoexcitation process of perovskite film can be obtained from the dynamics diagram of perovskite carrier. The excitation time of perovskite film of free-2D is 1420 fs, and after modification by PEABr, the excitation decay time of perovskite film is reduced to 1132 fs. Pump photoexcitation of the upper surface of perovskite, due to the presence of 2D, makes the overall carrier excitation time shorter, which means that the internal carrier excitation due to 2D/3D perovskite films is easier. For the subsequent electron extraction and transport process, the presence of 2D perovskite changes the energy level and morphology of the perovskite interface, making electron transport easier. It can be found from the carrier dynamic map that the carrier decay time of 2D/3D perovskite is longer than that of non-2D perovskite films, because 2D perovskite improves the interface defects of 3D perovskite. At the same time, the overall attenuation process of the carrier dynamics curve is also affected by the evolution process of 2D/3D heterojunction, which makes the carrier change more slowly. Then, as shown in **Fig. 2j** and **Fig. 2k**, the Photoluminescence spectroscopy (PL) tests were performed on target perovskite films with different storage times. The test results show that the fresh target perovskite film has an obvious low-dimensional perovskite peak of n=2 at the wavelength of 562 nm. Meanwhile, the main peak of the fresh (0 day) perovskite at the wavelength of 800 nm has a blue shift, and the main peak of the target perovskite film moved to a lower wavelength direction than the main peak of the control film. This indicates that the residual PEABr and the 2D/3D heterojunction has interfacial passivation effect on perovskite films. With the increase of the storage time, the peaks belonging to 2D perovskite disappeared, and the peaks of the target perovskite film began to slowly move to a higher wavelength, which indicate that the passivation effect of PEABr was gradually weakened. The perovskite peaks of the fresh (0 day) target perovskite films were significantly higher than those of the control films, suggesting that the non-radiative recombination in the 2D/3D heterojunction perovskite films was effectively inhibited. At the same time, after the target perovskite film is placed on the heating table for different time, the main peak of perovskite shows a downward trend,

which means that the evolution process of the 2D/3D heterojunction influences the interface characteristics of perovskite. As shown in **Fig. 2l**, time-resolved photoluminescence spectroscopy (TRPL) was conducted on the 2D/3D heterojunction perovskite films to investigate their carrier lifetime. The detailed test results can be found in the **Tab. S2**. In general, the fast decay lifetime (τ_1) can be attributed to defect-induced non-radiative recombination, while the slow decay lifetime (τ_2) is associated with radiative recombination. Control and 2D/3D perovskite films have fast decay life (τ_1=6.3ns, τ_1=19.2ns) and slow decay life (τ_2=158.5ns, τ_2=211.2ns), the average carrier lifetime (τ_{ave}= 154.1ns, τ_{ave}= 205.2ns) can be seen the defect and charge recombination in perovskite. The significant increase of fast decay life and slow decay life means that the defect state density decreases significantly and the non-radiative charge recombination decreases. The increase in average carrier lifetime suggests that carriers in the 2D/3D heterojunction perovskite films can travel longer distances, and non-radiative recombination within these films is effectively suppressed, consistent with the PL test findings.

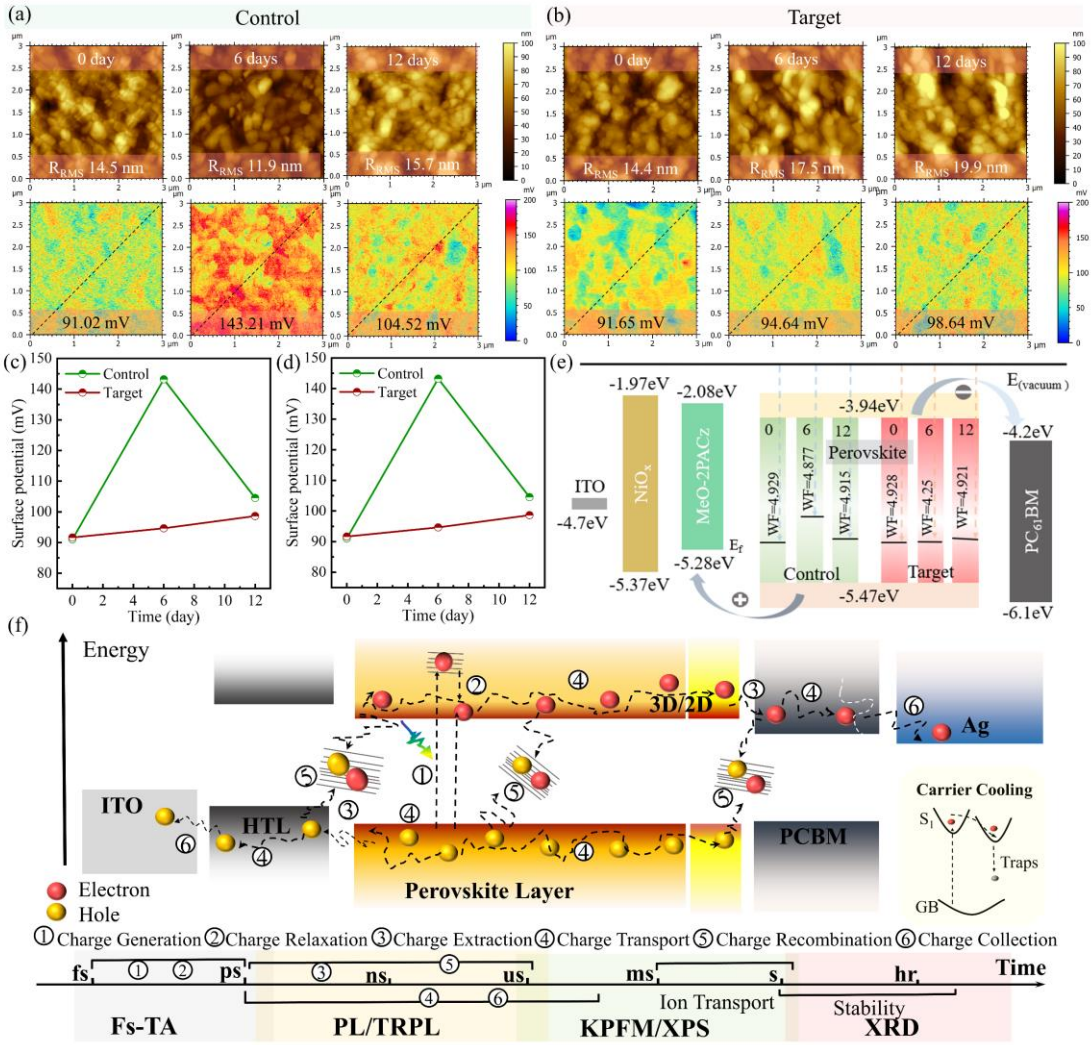

Figure 3. (a) AFM and KPFM diagram of control sample on a hot table at 60℃ for different time. (b) AFM and KPFM diagram of target sample on a hot table at 60℃ for different time. (c) RRMS profiles of control and target perovskite films. (d) Surface potential spectrogram of control and target perovskite films. (e) Work function variation diagram of control and target perovskite film. (f) Simulation diagram of carrier dynamic process and time scale behavior of perovskite.

Afterward, to further verify the process of surface change of the perovskite film, the atomic force microscopy (AFM) and kelvin probe force microscopy (KPFM) were used to test the perovskite film, as shown in **Fig. 3a** and **3b**. The root mean square (R_{RMS}) roughness data of the 2D/3D heterogeneous perovskite films with different heating times were obtained. The R_{RMS} difference between the control and target perovskite films (0 days) was not significant. However, the difference of R_{RMS} values between target film and control film further verified the existence of residual PEABr

and 2D perovskite on perovskite. The control perovskite film exhibited an R_{RMS} of 14.5 nm at 0 days, 11.9 nm at 6 days, and 15.7 nm at 12 days of storage. Conversely, the control perovskite film showed an R_{RMS} of 14.4 nm at 0 days, 17.5 nm at 6 days, and 19.9 nm at 12 days of storage. Meanwhile, the surface roughness of the control perovskite film after 12 days showed no difference compared to the film at 0 days, while the surface roughness of the target perovskite film increased gradually. However, the R_{RMS} value on the upper surface of the target perovskite film changes more gradually compared to the control perovskite film, significantly impacting the stability of PSCs. This observation, coupled with previous test results, suggests that it may be attributed to the decomposition of 2D perovskites and the emergence of PbI_2 crystals, influencing the surface characteristics of the 2D/3D heterojunction perovskites. At the same time, the KPFM testing indicated minimal difference in surface potential between the upper surface of the freshly prepared (0 day) control and target perovskite films (data from the diagonal). However, it could be seen from the analysis of the overall image that the upper surface potential of the target perovskite film was more concentrated, which may be caused by the presence of residual PEABr and the 2D/3D heterojunction perovskite. Meanwhile, the residual PEABr and the 2D/3D heterojunction perovskite fill the low potential space at the original 3D perovskite interface, which makes the potential on the surface of the perovskite appear more uniform. Additionally, the KPFM test was conducted on a perovskite film placed on a 60°C hot platform for different time. While the surface potential of the control films exhibited significant fluctuations over time, that of the target perovskite films remained largely unchanged. The surface potential and R_{RMS} of the target perovskite film exhibited a gradual increasing trend, while those of the control perovskite film showed a pattern of initially decreasing and then increasing. As shown in **Fig. 3c**, the surface R_{RMS} changes of target and control perovskite films show a more gradual change in the surface R_{RMS} of 2D/3D perovskite films compared with control films. The surface potential variation diagram of the control and target perovskite film is shown in **Fig. 3d**. The surface potential of the control film fluctuates greatly. **Fig. 3e** shows the relationship between the surface work function and the energy band change of the control and target perovskite films. Since

the 2D content of the target perovskite film is very small, the energy level of the target perovskite is tentatively like that of the control perovskite film. Excessive fluctuation in the upper surface of the perovskite film during the 12 days placement period can be detrimental to the final PSCs stability. Around 6 days of the target device, the slow increase in surface potential and R_{RMS} may be linked to the evolution of the 2D/3D heterojunction, influenced by the appearance of PbI_2 crystals and the decomposition of 2D perovskite, potentially compensating for perovskite film defects. **Fig. 3f** shows the entire carrier dynamic behavior relationship of perovskite. The behavior of photoexcited carrier between the interface of perovskite is affected by the defects in the perovskite and the carrier transport path. The carrier in perovskite film will undergo non-radiative recombination between perovskite film and perovskite interface, resulting in the quenching of the carrier. The carrier transport between interfaces will also be affected by the defect states and the energy level matching relationship between the interfaces. Therefore, the evolution of 2D/3D heterojunction is related to the behavior of perovskite carrier dynamics. Carriers transition from the ground state to the excited state by optical excitation, and then naturally return from the excited state to the ground state or are trapped by defects. This process of high-energy carrier return to the ground state can be described by carrier cooling. Because the process of carrier generation and transfer occurs very quickly, it will show different dynamics at different time scales. We use corresponding test methods to study the evolution of 2D/3D heterojunctions and the dynamic behavior changes of charge carriers. The evolution process of 2D/3D heterojunction has great influence on the stability of perovskite, and the fluctuation of perovskite interface can cause the change of carrier dynamics.

2.2 Analysis of perovskite films and devices

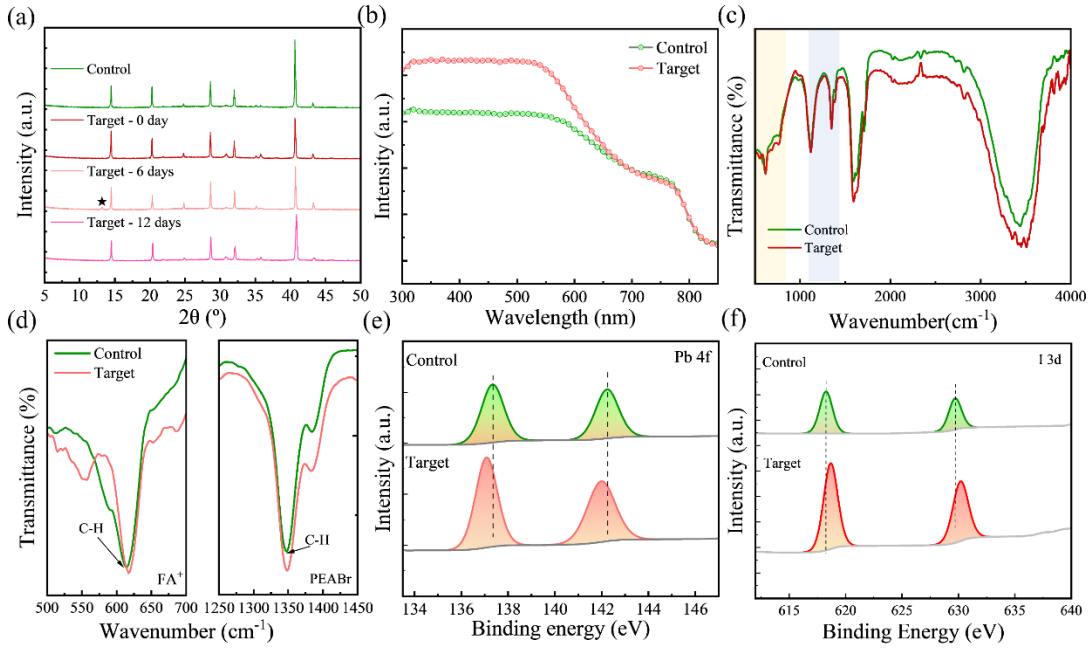

Figure 4. (a) XRD diagram of control and target perovskite films placed on the 60°C hot platform for different times. (b) UV-vis absorption spectra of perovskite films with ITO substrate. (c) FTIR diagram of perovskite films with ITO substrate. (d) FTIR diagram of perovskite films with 500 cm^{-2} to 1500 cm^{-2} wavenumber. (e, f) XPS diagram of perovskite films with ITO substrate.

To investigate the changes that occur on the surface of perovskite films during extended annealing processes, perovskite films with varying annealing durations underwent X-ray diffraction (XRD) tests (**Fig. 4a**). On the initial day (0 day), the target perovskite film demonstrates a more pronounced signal at the α phase peak of 14.5° in contrast to the control film. This suggests that the α phase perovskite crystals in the target film are more oriented along the (001) direction. The better crystallization of the perovskite also indicates that the presence of the 2D/3D heterojunction can better protect the crystals inside the 3D perovskite. At the same time, the δ phase diffraction peak intensity of the target film at 42° is lower than that of the control perovskite film, which indicates that the presence of the 2D/3D heterojunction can improve the stability of 3D perovskite phase. The film subjected to 60°C on a hot platform for 6 days simultaneously exhibited a weak PbI_2 peak at 12.4°, consistent with SEM results. As storage time increased, the PbI_2 peak diminished, while the δ phase peak continued to decrease. The observed PEABr escape during storage appears beneficial for the overall

perovskite film. Furthermore, the stability of the target perovskite film (001) peak suggests that PEABr escape does not significantly affect the bulk phase of the perovskite. Subsequently, the ultraviolet-visible (UV-vis) spectrophotometer tests were conducted on the control and target perovskite samples. As shown in **Fig. 4b**, the visible light absorption range of the target perovskite film is lower than that of the control perovskite film. This disparity may arise from alterations in the band gap of the target perovskite film due to the presence of the 2D perovskite and residual PEABr. Then, as shown in **Fig. S6**, the optical band gap of both the control and target films was calculated using ultraviolet data. The results indicate that the optical band gap of the perovskite film increases from 1.524 eV to 1.529 eV due to the presence of the 2D perovskite and PEABr. However, between 300 nm and 550 nm, the visible light absorption capacity of the target film shows a notable improvement compared to the control film, indicating a reduction in non-radiative recombination in the surface of the target perovskite film. At the same time, the 2D perovskite can improve the band gap of perovskite, which has been demonstrated in previous studies. Ziqi Liang et al found that the band gap of the 2D perovskite is usually higher than that of the 3D perovskite solar cells [37]. Therefore, for two-dimensional passivation layers prepared with PEABr, it is a normal phenomenon that the band gap of perovskite films is improved. The increase in the perovskite band gap also provides direct evidence for the increase in the open circuit voltage (V_{OC}) of the final device. To further investigate the changes in internal bonding atoms within the control and target perovskite films, Fourier-transform infrared spectroscopy (FTIR) was conducted, as depicted in **Fig. 4c**. It can be found that the N-H stretching vibration absorption wavelength in perovskite moves from 3440 cm^{-1} to 3515 cm^{-1}, while the vibration absorption wavelength of C=N moves from 1590 cm^{-1} to 1596 cm^{-1}. The wavelength of N-H and C=N bond moves to higher wavelength, which indicates that PEABr has certain induction effect on perovskite molecules in perovskite films. The **Fig. 4d** shows the low wave number amplification in the FTIR graph. From the test results, it can be inferred that the bending vibration absorption wavelength of the C-H bond in the perovskite component ranges from 615 cm^{-1} to 617 cm^{-1}, whereas the bending vibration absorption wavelength of the C-H bond in PEABr

ranges from 1347 cm^{-1} to 1349 cm^{-1}. The C-H bond in the FA^+ and the C-H bond in the PEABr oscillate simultaneously, indicating the interaction between PEABr and FA^+. At the same time, as shown in **Fig. 4e** and **4f**, X-ray photoelectron spectroscopy (XPS) analysis was conducted on the target and control perovskite films to investigate changes in element binding energy peaks on their surfaces. The fitting results revealed that in the target perovskite film, the Pb^{4f} peak shifted towards lower binding energy, suggesting that the presence of PEABr altered the environment surrounding Pb ions, promoting their binding with FA^+. The shift of the I^{3d} peak towards higher binding energy in the target perovskite film indicates reduced reactivity of I ions within the perovskite structure, thereby potentially lowering the defect density attributed to iodine ions. Combining the previous FTIR test results and the molecular electrostatic potential results of PEABr, the PEA^+ ions can interact with I element, thus affecting the existence form of I element, and the Br^- can interact with Pb element, thus changing some of the action characteristics of Pb element. Meanwhile, the full peak of XPS test results is shown in **Fig. S7**. Since the control film does not contain Br element, the content of Br element in the target film is very small, so there is no strong peak of Br element in the XPS test results. These phenomena further show that the evolution process of the 2D/3D heterojunction is regular. In previous the 2D/3D studies it was found that 2D perovskites constructed using some special organic spacer molecules would diffuse to 3D perovskites. This diffusion process destroys the crystal structure of the 3D perovskite and causes severe ion migration and defect aggregation in the 3D perovskite. In this experiment, the 2D passivation layer constructed by the PEABr on the upper surface of the 3D perovskite will decompose and the PEABr molecules will separate on the upper surface of the perovskite film over time, because the characteristics of Br^- make it migrate to the upper surface of perovskite during the process of ion migration.

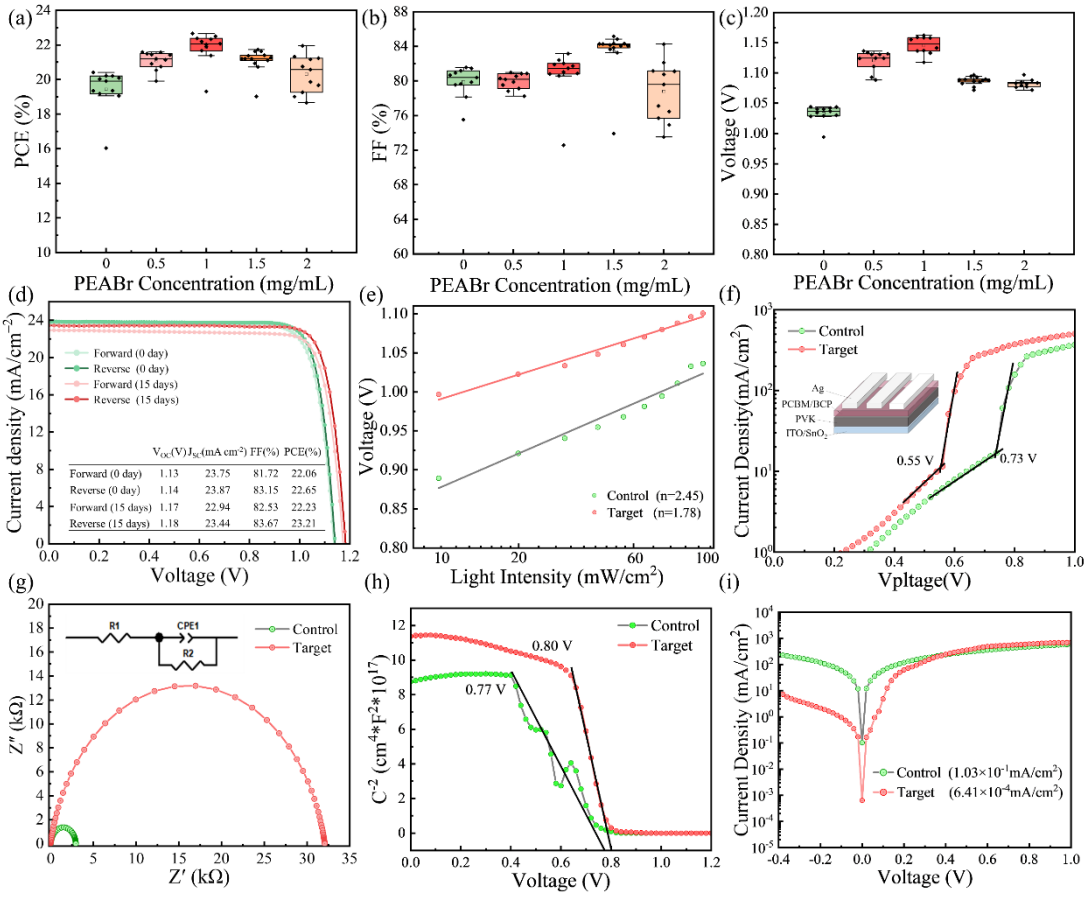

Figure 5. (a-c) Photovoltaic performance diagram of control and target devices. (d) J-V diagram of 0.105 cm^2 fresh device and after 15 days device in N_2 boxes at normal temperature. (e) Light intensity dependence test diagram between control and target devices. (f) SCLC test diagram of control and target devices. (g) EIS diagram of the control and target devices. (h) Mott-Schottky diagram of control and target devices. (i) Dark current test diagram of control and target devices.

In this experiment, the final prepared device structure is shown in supplementary **Fig. S8.** By spinning PEABr on the upper surface of 3D perovskite as the passivation interface layer of perovskite, the PEABr can construct 2D perovskite layer on the upper surface of 3D perovskite and form the 2D/3D heterostructures. The 2D/3D heterojunction PSCs constructed using this method have significantly improved performance and stability compared to pure 3D perovskite. First, as shown in **Fig. 5a-c** and supplementary **Fig. S9**, the open circuit voltage (V_{OC}) and fill factor (FF) of the target device with the PEABr and the 2D/3D heterojunction are greatly improved. The highest PCE of the prepared 0.105cm^2 PSCs reaches 22.65% (the detailed data are shown in **Tab. S3**). The PCE of target device increase is 2.07% compared to the control

device. Meanwhile, as shown in supplementary **Fig. S10**, the highest PCE of the prepared 1cm^2 PSCs reaches 20.45% and the hysteresis of the HI is 0.013. Finally, the J-V diagram of the optimal device and in N_2 boxes at normal temperature after 15 days devices is shown in **Fig. 5d**. The device efficiency increased from 22.65% to 23.21% after 15 days of storage, with the largest change due to the increase in open circuit voltage from 1.14 V to 1.18 V, which may be caused by the presence of PbI_2 crystals in 2D/3D heterojunction. To verify the accuracy of our device test efficiency, we conducted external quantum efficiency (EQE) tests (**Fig. S11**) on the control and target devices. It was observed that the light absorption images of the target and the control device were essentially identical at various wavelengths. Additionally, the final integration current density indicated that there was not a significant difference in the current between the target device and the control device. However, the integration current density of the target device is 1.08 mAcm^{-2} higher than the J-V test current, and the integrated current density of the control device is 0.18 mAcm^{-2} higher than the J-V current. The error between the EQE Integrating current and the J-V current is less than 4%, which indicates that the J-V test current is consistent with the actual efficiency of PSCs. Then, we tested the dependence of the light intensity of the device, and the test results were shown in **Fig. 5e**. Meanwhile, the ideal factor obtained from the linear fitting of the test data for the final target device is 1.78, which is 0.67 lower than that of the control device. This indicates that the 2D/3D heterojunction perovskites exhibit lower non-radiative recombination and superior carrier transport capability. Under the same conditions, the 2D/3D heterojunction effectively inhibits carrier recombination in the target device. This is due to the interfacial passivation of 2D perovskite and PEABr on perovskite film, which reduces the surface defect density of perovskite. Moreover, this optimization improves the charge transport mechanics at the interface. To investigate the variation of defect density in perovskite films, as shown in **Fig. 5f**, the space charge-limited current (SCLC) measurements on PSCs electron-only devices are performed. The electron-only devices structure in the image is the device for our test of the SCLC. The defect density in perovskite films can be calculated by formula 3 based on the SCLC test results. Where V_{TFL} is the starting voltage of the trap filling limit, L

is the thickness of the active layer, ε is the relative perovskite dielectric constant, e is the basic charge and ε_0 is the vacuum dielectric constant. Then, the defect starting voltage of the control with the target PSCs is 0.55 V and 0.73 V. The decrease of the defect starting voltage means that the defect density of the device is lower, and it can also prove that the carrier recombination of the target device is suppressed.

$$N_t = \frac{2\varepsilon_0 \varepsilon V_{TFL}}{eL^2} \quad \text{(formula 3)}$$

The electrochemical impedance spectroscopy (EIS) test results are shown in **Fig. 5g**. In our device test, both the control and target devices showed a particularly small internal resistance R_0, the size of which is close to 0 Ω, so it is very small in the image, and there is basically no difference. However, the electrochemical impedance fitting radius of the 2D/3D heterojunction perovskite devices is larger than that of control devices. The increase in charge transfer resistance means that carrier transport of PSCs is more difficult. However, due to the presence of the 2D/3D heterojunction, the target perovskite film has better light absorption capacity, so the final device is more efficient. At the same time, as shown in **Fig. 5h**, to explore the differences in internal electric fields of the 2D/3D heterojunction devices with higher charge transfer resistance, the Mott-Schottky tests were carried out on the devices. The test results show that the internal electric field (V_{bi}) of the target device is 0.80 V and that of the control device is 0.77 V. The higher V_{bi} of the target device means that the driving force of charge separation is enhanced, which is conducive to carrier transport [38]. Finally, we placed the device in a completely dark environment to test the dark current of the device (shown in **Fig. 5i**). The results reveal that the dark current density of the control device is 1.03×10^{-1} mA/cm^2, whereas that of the target device is 6.41×10^{-4} mA/cm^2. The dark current of the target device is lower than that of the control device, suggesting that the incorporation of the 2D/3D heterojunction perovskite and the residual PEABr in the target device exerts a mitigating effect on the generation of leakage current.

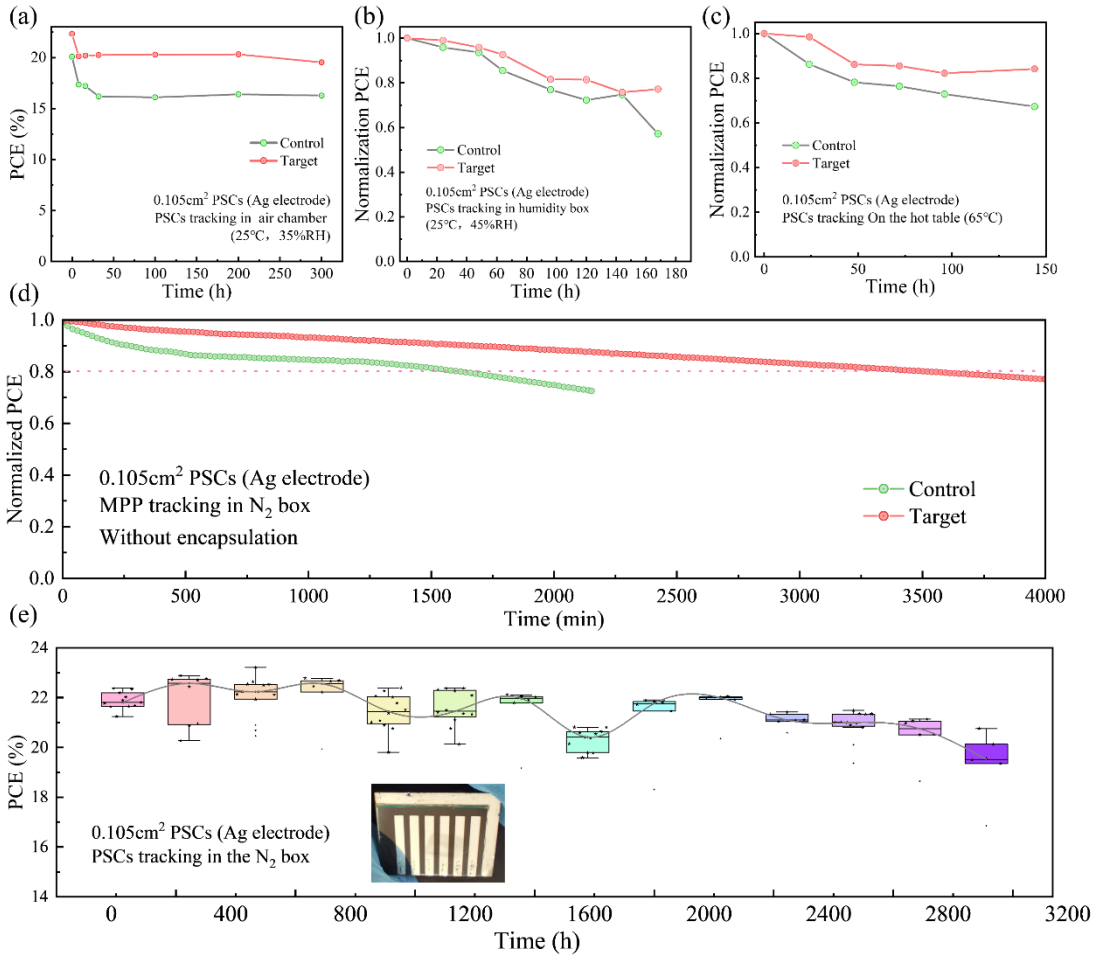

Figure 6. (a) Unpackaged devices are tested for stability when placed in air at 25℃ and 35%RH. (b) Unpackaged devices are placed in a constant humidity chamber at 25℃ and 45%RH for stability testing. (c) Stability testing of unpackaged devices on a hot table at 65℃. (d) MPP tracking test of unpackaged devices in the N_2 box. (e) Stability test of optimal device in normal temperature N_2 atmosphere.

The stability of PSCs is an important difficulty, so the stability test of the final device is an essential part. Next, the stability of the device is tested by the control device and the target device in various test environments. B. P. Kore et al studied three organic cations with different alkyl chain lengths, and used 2D perovskite as the encapsulation layer on top of 3D perovskite [39]. When the perovskite film is completely immersed in water, it can remain in water for 3 minutes, which means that the hydrophobicity of the perovskite film is significantly enhanced. Therefore, using 2D perovskite to improve the stability of the 3D perovskite is a promising method. Next, the stability of the target device and the control device will be tested. As shown in **Fig. 6a**, we placed the control

and the target device in the air (25℃, 35%RH), and the results showed that the stability of the target device was greatly improved compared with that of the control device. Upon storage in ambient air for a specified duration, the efficiency of the control device exhibited considerable variability, declining by 4% over the course of a single day. However, the target device efficiency experienced a mere 2% decrease, with any subsequent fluctuations being notably minimal. This stability improvement, we believe that 2D/3D perovskite and PEABr play an effective role in inhibiting the defects of the device. However, we did not observe a tendency of increase in the efficiency of the target device under these conditions, and we speculate that this is the 2D/3D heterojunction changes too quickly under the influence of humidity. As shown in **Fig. 6b**, the same batch of devices was placed in a constant humidity chamber at 45%RH, and the efficiency of the control devices decreased by 80% after 60 hours. Secondly, the same batch of devices is placed on a hot table at 65°C for a temperature stability test (**Fig. 6c**), and the device efficiency decreased significantly, possibly due to the oxidation of the Ag electrode. However, the stability of the target device was still higher than that of the control device. In various storage stability tests, the stability of the target device is stronger than that of the control device, which indicates that the interface action of the PEABr and 2D/3D perovskite pair is worthy of attention.

Finally, the maximum power point (MPP) tracking test on the PSCs with Ag electrode was conducted (**Fig. 6d**), and the test results indicated that the efficiency of the target device decreased to 80% after 3500 minutes of continuous testing. This was a particularly surprising result in MPP tests of PSCs using Ag electrodes. As shown in **Fig. 6e**, the optimal PSCs is stored in the N_2 box for stability testing. The results showed that the efficiency of the target PSCs continued to increase (from 22.65% to 23.21%) after 300 hours of storage, a phenomenon rarely observed in the study of inverted PSCs. Simultaneously, this phenomenon is observable due to the relatively slow degradation of the PSCs within the N_2 environment. Furthermore, the notable enhancement in initial stability of the 2D/3D heterojunction perovskite is closely linked to the evolution of the respective film structures. Notably, the device maintains 89% of its initial efficiency after 3000 hours in the N_2 box, marking exceptionally high stability data for PSCs

employing silver electrodes. Detailed test data is shown in supplementary **Tab. S4**. This test result shows that the change of PEABr and the 2D/3D heterojunction on the upper surface of perovskite is beneficial for the stability of the PSCs.

3.Conclusion

In our research, we discovered that in the 2D/3D heterojunction PSCs tends to degrade over time during the operation. Additionally, the organic spacer molecules (PEABr) within the 2D perovskite lattice are separated from the upper surface of the perovskite during its long-term operation. In this separation process, the PbI_2 crystals will appear on the upper surface of the 2D/3D heterojunction perovskite film, which improves the carrier transport capacity at the interface and reduces the non-radiative recombination at the interface. In addition, by using optical characterization such as TA and PL to analyse the evolution process of 2D/3D, the carrier dynamic behaviour relationship corresponding to the evolution process is obtained. The V_{OC} of the PSCs increased from 1.14 V to 1.18 V and the PCE increased to 23.21% after the PSCs placed in the N_2 box for 300 hours. Finally, the unpackaged devices maintained 89% of their initial performance for 3000 hours in a room temperature N_2 box. Our work provides insights into the evolution mechanism of the 2D/3D heterojunctions and has important implications for tuning the 2D/3D structures and improving PSCs performance and stability.

Acknowledgements

We would like to express our sincere appreciation for the generous financial support provided by the Sichuan Science and Technology Program (No. 2022NSFSC0226) and Sichuan Science and Technology Program (No. 2023ZYD0163), the Production-Education Integration Demonstration Project of Sichuan Province, the Photovoltaic Industry Production-Education Integration Comprehensive Demonstration Base of Sichuan Province (Sichuan Financial Education [2022] No.106), China Tianfu Yongxing Laboratory Science and Technology Key Project (2023KJGG15), National Key Research and Development Program of China (2022YFB3803300) and Beijing Natural Science Foundation (IS23037).

Acknowledges the Department for Energy Security and Net Zero (project ID: NEXTCCUS) and the ACT program (Accelerating CCS Technologies, Horizon2020 project NO. 691712).

References

[1] Y. Liu, S. Yuan, H. Zheng, M. Wu, S. Zhang, J. Lan, W. Li, J. Fan, Structurally Dimensional Engineering in Perovskite Photovoltaics, Advanced Energy Materials 13 (2023) 2300188.

[2] E. Ruggeri, S.D. Stranks, E. Manidakis, C.C. Stoumpos, C. Katan, Halide Perovskites: Low Dimensions for Devices, ACS Energy Letters 4 (2019) 2902-2904.

[3] C. Zuo, L. Ding, Drop-Casting to Make Efficient Perovskite Solar Cells under High Humidity, Angewandte Chemie International Edition 60 (2021) 11242-11246.

[4] A. Kojima, K. Teshima, Y. Shirai, T. Miyasaka, Organometal Halide Perovskites as Visible-Light Sensitizers for Photovoltaic Cells, Journal of the American Chemical Society 131 (2009) 6050-6051.

[5] H. Chen, C. Liu, J. Xu, A. Maxwell, W. Zhou, Y. Yang, Q. Zhou, A.S.R. Bati, H. Wan, Z. Wang, L. Zeng, J. Wang, P. Serles, Y. Liu, S. Teale, Y. Liu, M.I. Saidaminov, M. Li, N. Rolston, S. Hoogland, T. Filleter, M.G. Kanatzidis, B. Chen, Z. Ning, E.H. Sargent, Improved Charge Extraction in Inverted Perovskite Solar Cells with Dual-site-binding Ligands, Science 384 (2024) 189-193.

[6] S. Sidhik, Y. Wang, M. De Siena, R. Asadpour, A.J. Torma, T. Terlier, K. Ho, W. Li, A.B. Puthirath, X. Shuai, A. Agrawal, B. Traore, M. Jones, R. Giridharagopal, P.M. Ajayan, J. Strzalka, D.S. Ginger, C. Katan, M.A. Alam, J. Even, M.G. Kanatzidis, A.D. Mohite, Deterministic Fabrication of 3D/2D Perovskite Bilayer Stacks for Durable and Efficient Solar Cells, Science 377 (2022) 1425-1430.

[7] I. Metcalf, S. Sidhik, H. Zhang, A. Agrawal, J. Persaud, J. Hou, J. Even, A.D. Mohite, Synergy of 3D and 2D Perovskites for Durable, Efficient Solar Cells and Beyond, Chemical Reviews 123 (2023) 9565-9652.

[8] L. Luo, H. Zeng, Z. Wang, M. Li, S. You, B. Chen, A. Maxwell, Q. An, L. Cui, D. Luo, J. Hu, S. Li, X. Cai, W. Li, L. Li, R. Guo, R. Huang, W. Liang, Z.-H. Lu, L. Mai, Y. Rong, E.H. Sargent, X. Li, Stabilization of 3D/2D Perovskite Heterostructures Via Inhibition of Ion Diffusion by Cross-linked Polymers for Solar Cells with Improved Performance, Nature Energy 8 (2023) 294-303.

[9] A.R.b.M. Yusoff, M.K. Nazeeruddin, Low-Dimensional Perovskites: From Synthesis to Stability in Perovskite Solar Cells, Advanced Energy Materials 8 (2018) 1702073.

[10] J. Gu, X. Sun, P. F. Chan, X. Lu, P. Zeng, J. Gong, F. Li, M. Liu, Constructing Low-dimensional Perovskite Network to Assist Efficient and Stable Perovskite Solar Cells, Journal of Energy Chemistry, 96 (2024) 625-632.

[11] P. Chen, Y. Bai, S. Wang, M. Lyu, J.-H. Yun, L. Wang, In Situ Growth of 2D Perovskite Capping Layer for Stable and Efficient Perovskite Solar Cells, Advanced Functional Materials 28 (2018) 1706923.

[12] E.-B. Kim, M.S. Akhtar, H.-S. Shin, S. Ameen, M.K. Nazeeruddin, A Review on Two-dimensional (2D) and 2D-3D Multidimensional Perovskite Solar Cells: Perovskites Structures, Stability, and Photovoltaic Performances, Journal of Photochemistry and Photobiology C: Photochemistry Reviews 48 (2021) 100405.
[13] G. Uzurano, N. Kuwahara, T. Saito, K. Abe, S. Miyake, D. Hishida, Y. Takeoka, A. Fujii, M. Ozaki, 2D/3D Perovskite Heterostructure Solar Cell with Orientation-controlled Dion–Jacobson 2D Phase, Applied Physics Express 16 (2023) 041005.
[14] P. Li, Y. Zhang, C. Liang, G. Xing, X. Liu, F. Li, X. Liu, X. Hu, G. Shao, Y. Song, Phase Pure 2D Perovskite for High-Performance 2D–3D Heterostructured Perovskite Solar Cells, Advanced Materials 30 (2018) 1805323.
[15] C.W. Jang, H. Kim, M.K. Nazeeruddin, D.H. Shin, S.-H. Choi, Piezo-electric and -Phototronic Effects of Perovskite 2D/3D Heterostructures, Nano Energy 84 (2021) 105899.
[16] M.A. Mahmud, T. Duong, J. Peng, Y. Wu, H. Shen, D. Walter, H.T. Nguyen, N. Mozaffari, G.D. Tabi, K.R. Catchpole, K.J. Weber, T.P. White, Origin of Efficiency and Stability Enhancement in High-Performing Mixed Dimensional 2D-3D Perovskite Solar Cells: A Review, Advanced Functional Materials 32 (2022) 2009164.
[17] D. Gao, B. Li, Z. Li, X. Wu, S. Zhang, D. Zhao, X. Jiang, C. Zhang, Y. Wang, Z. Li, N. Li, S. Xiao, W.C.H. Choy, A.K.Y. Jen, S. Yang, Z. Zhu, Highly Efficient Flexible Perovskite Solar Cells through Pentylammonium Acetate Modification with Certified Efficiency of 23.35%, Advanced Materials 35 (2023) 2206387.
[18] M. Xiong, W. Zou, K. Fan, C. Qin, S. Li, L. Fei, J. Jiang, H. Huang, L. Shen, F. Gao, A.K.Y. Jen, K. Yao, Tailoring Phase Purity in the 2D/3D Perovskite Heterostructures Using Lattice Mismatch, ACS Energy Letters 7 (2022) 550-559.
[19] X. Dong, Y. Tang, Y. Li, X. Li, Y. Zhao, W. Song, F. Wang, S. Xu, Y. Zhou, C. Ran, Z. Miao, L. Song, Z. Wu, Boosting MA-based Two-dimensional Ruddlesden-Popper perovskite Solar Cells by Incorporating A Binary Spacer, Journal of Energy Chemistry, 95 (2024) 348-356.
[20] C. Li, R. Zhu, Z. Yang, J. Lai, J. Tan, Y. Luo, S. Ye, Boosting Charge Transport in a 2D/3D Perovskite Heterostructure by Selecting an Ordered 2D Perovskite as the Passivator, Angewandte Chemie International Edition 62 (2023) e202214208.
[21] P. Sebastia-Luna, U. Pokharel, B.A.H. Huisman, L.J.A. Koster, F. Palazon, H.J. Bolink, Vacuum-Deposited Cesium Tin Iodide Thin Films with Tunable Thermoelectric Properties, ACS Applied Energy Materials 5 (2022) 10216-10223.
[22] J. Qian, J. He, Q. Zhang, C. Zhu, S. Chen, Z. Wei, X. Leng, Z. Zhou, B. Shen, Y. Peng, Q. Niu, S. Yang, Y. Hou, Minimizing Interfacial Energy Losses in Inverted Perovskite Solar Cells by A Dipolar Stereochemical 2D Perovskite Interface, Journal of Energy Chemistry, 90 (2024) 496-503.
[23] J. Duan, Y. Zhao, B. He, Q. Tang, High-Purity Inorganic Perovskite Films for Solar Cells with 9.72 % Efficiency, Angewandte Chemie International Edition 57 (2018) 3787-3791.
[24] T. Niu, Y.-M. Xie, Q. Xue, S. Xun, Q. Yao, F. Zhen, W. Yan, H. Li, J.-L. Brédas, H.-L. Yip, Y. Cao, Spacer Engineering of Diammonium-Based 2D Perovskites

toward Efficient and Stable 2D/3D Heterostructure Perovskite Solar Cells, Advanced Energy Materials 12 (2022) 2102973.
[25] B.R. Wygant, A.Z. Ye, A. Dolocan, Q. Vu, D.M. Abbot, C.B. Mullins, Probing the Degradation Chemistry and Enhanced Stability of 2D Organolead Halide Perovskites, Journal of the American Chemical Society 141 (2019) 18170-18181.
[26] L. Gao, P. Hu, S. Liu, Low-dimensional Perovskite Modified 3D Structures for Higher-performance Solar Cells, Journal of Energy Chemistry, 81(2023) 389-403.
[27] A.A. Sutanto, R. Szostak, N. Drigo, V.I.E. Queloz, P.E. Marchezi, J.C. Germino, H.C.N. Tolentino, M.K. Nazeeruddin, A.F. Nogueira, G. Grancini, In Situ Analysis Reveals the Role of 2D Perovskite in Preventing Thermal-Induced Degradation in 2D/3D Perovskite Interfaces, Nano Letters 20 (2020) 3992-3998.
[28] X. Zhang, W. Zhou, X. Chen, Y. Chen, X. Li, M. Wang, Y. Zhou, H. Yan, Z. Zheng, Y. Zhang, Dual Optimization of Bulk and Surface via Guanidine Halide for Efficient and Stable 2D/3D Hybrid Perovskite Solar Cells, Advanced Energy Materials 12 (2022) 2201105.
[29] W. Zhou, L. Jia, M. Chen, X. Li, Z. Su, Y. Shang, X. Jiang, X. Gao, T. Chen, M. Wang, Z. Zhu, Y. Lu, S. Yang, An Improbable Amino-Functionalized Fullerene Spacer Enables 2D/3D Hybrid Perovskite with Enhanced Electron Transport in Solar Cells, Advanced Functional Materials 32 (2022) 2201374.
[30] H. Li, C. Zhang, C. Gong, D. Zhang, H. Zhang, Q. Zhuang, X. Yu, S. Gong, X. Chen, J. Yang, X. Li, R. Li, J. Li, J. Zhou, H. Yang, Q. Lin, J. Chu, M. Grätzel, J. Chen, Z. Zang, 2D/3D Heterojunction Engineering at the Buried Interface Towards High-Performance Inverted Methylammonium-free Perovskite Solar Cells, Nature Energy 8 (2023) 946-955.
[31] R. Azmi, E. Ugur, A. Seitkhan, F. Aljamaan, A.S. Subbiah, J. Liu, G.T. Harrison, M.I. Nugraha, M.K. Eswaran, M. Babics, Y. Chen, F. Xu, T.G. Allen, A.u. Rehman, C.-L. Wang, T.D. Anthopoulos, U. Schwingenschlögl, M. De Bastiani, E. Aydin, S. De Wolf, Damp Heat–stable Perovskite Solar Cells with Tailored-dimensionality 2D/3D Heterojunctions, Science 376 (2022) 73-77.
[32] Y. Bai, Z. Huang, X. Zhang, J. Lu, X. Niu, Z. He, C. Zhu, M. Xiao, Q. Song, X. Wei, C. Wang, Z. Cui, J. Dou, Y. Chen, F. Pei, H. Zai, W. Wang, T. Song, P. An, J. Zhang, J. Dong, Y. Li, J. Shi, H. Jin, P. Chen, Y. Sun, Y. Li, H. Chen, Z. Wei, H. Zhou, Q. Chen, Initializing Film Homogeneity to Retard Phase Segregation for Stable Perovskite Solar Cells, Science 378 (2022) 747-754.
[33] X. Liu, D. Luo, Z.-H. Lu, J.S. Yun, M. Saliba, S.I. Seok, W. Zhang, Stabilization of Photoactive Phases for Perovskite Photovoltaics, Nature Reviews Chemistry 7 (2023) 462-479.
[34] S. Masi, A.F. Gualdrón-Reyes, I. Mora-Seró, Stabilization of Black Perovskite Phase in $FAPbI_3$ and $CsPbI_3$, ACS Energy Letters 5 (2020) 1974-1985.
[35] T. Mahmoudi, Y. Wang, Y.-B. Hahn, Stability Enhancement in Perovskite Solar Cells with Perovskite/Silver–Graphene Composites in the Active Layer, ACS Energy Letters 4 (2019) 235-241.
[36] Z. Yang, B. Cai, B. Zhou, T. Yao, W. Yu, S. Liu, W.-H. Zhang, C. Li, An Up-scalable Approach to $CH_3NH_3PbI_3$ Compact Films for High-Performance

Perovskite Solar Cells, Nano Energy 15 (2015) 670-678.
[37] Y. Lei, Y. Zhang, J. Huo, F. Ding, Y. Yan, Y. Shen, X. Li, W. Kang, Z. Yan, Stability Strategies and Applications of Iodide Perovskites, Small (2024) 2311880.
[38] Z. Huang, Z. Ma, C. Deng, T. Yu, G. Li, Z. Du, W. You, J. Yang, Y. Chen, Y. Li, S. Hou, Q. Yang, Q. Zhang, H. Du, Y. Li, H. Shu, Q. Liu, C. Peng, Y. Huang, J. Yu, Y. Lin, K. Sun, W. Long, Aging-Resistant Precursor with Ultrawide Annealing Window for 24.08% Perovskite Solar Cells, Advanced Energy Materials 14 (2024) 2302769.
[39] J. Zhang, S. Langner, J. Wu, C. Kupfer, L. Lüer, W. Meng, B. Zhao, C. Liu, M. Daum, A. Osvet, N. Li, M. Halik, T. Stubhan, Y. Zhao, J.A. Hauch, C.J. Brabec, Intercalating-Organic-Cation-Induced Stability Bowing in Quasi-2D Metal-Halide Perovskites, ACS Energy Letters 7 (2022) 70-77.
[40] P. Li, Y. Zhang, C. Liang, G. Xing, X. Liu, F. Li, X. Liu, X. Hu, G. Shao, Y. Song, Phase Pure 2D Perovskite for High-Performance 2D/3D Heterostructured Perovskite Solar Cells, Advanced Materials 30 (2018) 1805323.
[41] Y. Lv, D. Si, X. Song, K. Wang, S. Wang, Z. Zhao, C. Hao, L. Wei, Y. Shi, Pseudohalogen-Based 2D Perovskite: A More Complex Thermal Degradation Mechanism Than 3D Perovskite, Inorganic Chemistry 57 (2018) 2045-2050.
[42] Z. Wang, Q. Ou, Y. Zhang, Q. Zhang, H.Y. Hoh, Q. Bao, Degradation of Two-Dimensional $CH_3NH_3PbI_3$ Perovskite and $CH_3NH_3PbI_3$/Graphene Heterostructure, ACS Applied Materials & Interfaces 10 (2018) 24258-24265.
[43] Q. Liu, Z. Ma, Y. Li, G. Yan, D. Huang, S. Hou, W. Zhou, X. Wang, J. Ren, Y. Xiang, R. Ding, X. Yue, Z. Du, M. Zhang, W. Zhang, L. Duan, Y. Huang, Y. Mai, Heterogeneous Lead Iodide Obtains Perovskite Solar Cells with Efficiency of 24.27%, Chemical Engineering Journal 448 (2022) 137676.
[44] Y. Liu, H. Zhou, Y. Ni, J. Guo, R. Lu, C. Li, X. Guo, Revealing Stability Origin of Dion-Jacobson 2D Perovskites with Different-Rigidity Organic Cations, Joule 7 (2023) 1016-1032.
[45] Y. Zhong, G. Liu, Y. Su, W. Sheng, L. Gong, J. Zhang, L. Tan, Y. Chen, Diammonium Molecular Configuration-Induced Regulation of Crystal Orientation and Carrier Dynamics for Highly Efficient and Stable 2D/3D Perovskite Solar Cells, Angewandte Chemie International Edition 61 (2022) e202114588.
[46] G. Grancini, C. Roldán-Carmona, I. Zimmermann, E. Mosconi, X. Lee, D. Martineau, S. Narbey, F. Oswald, F. De Angelis, M. Graetzel, M.K. Nazeeruddin, One-Year Stable Perovskite Solar Cells by 2D/3D Interface Engineering, Nature Communications 8 (2017) 15684.
[47] X. Jiang, J. Zhang, S. Ahmad, D. Tu, X. Liu, G. Jia, X. Guo, C. Li, Dion-Jacobson 2D-3D Perovskite Solar Cells with Improved Efficiency and Stability, Nano Energy 75 (2020) 104892.
[48] F. Wang, X. Jiang, H. Chen, Y. Shang, H. Liu, J. Wei, W. Zhou, H. He, W. Liu, Z. Ning, 2D-Quasi-2D-3D Hierarchy Structure for Tin Perovskite Solar Cells with Enhanced Efficiency and Stability, Joule 2 (2018) 2732-2743.
[49] Q. Lai, R. Zhuang, K. Zhang, T. Wu, L. Xie, R. Zhao, L. Yang, Y. Wang, Y. Hua,

A Multifunctional Liquid Crystal as Hole Transport Layer Additive Enhances Efficiency and Stability of Perovskite Solar Cells, Angewandte Chemie International Edition, 62 (2023) e202305670.
[50] A.D. Wright, C. Verdi, R.L. Milot, G.E. Eperon, M.A. Pérez-Osorio, H.J. Snaith, F. Giustino, M.B. Johnston, L.M. Herz, Electron-Phonon Coupling in Hybrid Lead Halide Perovskites, Nature Communications 7 (2016) 11755.

Highlights

The evolution mechanism of 2D/3D heterojunction was firstly proposed.

The relationship between the evolution mechanism of 2D/3D heterojunction and the stability of perovskite solar cell devices is systematically demonstrated.

Interface and carrier dynamics changes caused by evolution of 2D/3D heterojunctions based on ultrafast spectroscopy.